QUARTERLY OF APPLIED MATHEMATICS

Vol. XXIX JANUARY 1972 No. 4

"ESCAPE" FROM A POTENTIAL WELL (PART I)*

BY

R. SUBRAMANIAN AND R. E. KRONAUER

Harvard University

1. Introduction. The problem discussed in this paper has its origin in a paper "Dynamic buckling of elastic structures" by B. Budiansky [1]. In the course of formulating certain generalized criteria for dynamic buckling in [1] a conservative two-degree-of-freedom problem is considered where the potential energy function exhibits a topography shown in Fig. 1. A unit mass particle is located initially at the bottom of one of the two bowls and subjected to an initial velocity. The question is then what combination of initial velocity components will cause the particle to go over into the second bowl. Obviously the kinetic energy imparted must be at least equal to the saddle-point energy but much larger energies might be expected if the velocity were directed obliquely from the saddle direction.

The problem concerning escape from a potential well arises also in astronomy. Galactic models having a time-independent two-dimensional potential function and an axis of symmetry have been studied ([2] to [5]). In these papers the potential functions used permit escape for energies only slightly higher than that of the saddle point nearest to origin. The model developed here permits trapped motions in the potential well with energies far exceeding that of the nearest saddle point.

2. Model formulation. We will consider a Hamiltonian, H, for a system of two coordinates:

$$H = \frac{\dot{x}_1^2 + \dot{x}_2^2}{2} + V(x_1, x_2) = \frac{\dot{x}_1^2 + \dot{x}_2^2}{2} + 2x_2^2 + \frac{x_1^2}{2} + x_2^3 - \frac{\epsilon}{2}(\gamma x_1^2 x_2 + \nu x_1^2), \tag{2.1}$$

where $(\dot{})$ indicates time derivative, and the corresponding differential equations

$$(d^2x_1/dt^2) + x_1 = \epsilon(\nu x_1 + \gamma x_1 x_2), \tag{2.2a}$$

$$(d^2x_2/dt^2) + 4x_2 + 3x_2^2 = (\epsilon\gamma/2)x_1^2 . \tag{2.2b}$$

The parameter γ indicates the strength of the nonlinear coupling between (2.2a) and (2.2b). It is taken to be symmetric in x_1 for simplicity. To permit appreciable energy exchange for small-amplitude oscillations the linearized frequencies in the coordinates x_1, x_2 are taken in the ratio of 1:2. The parameter ν permits detuning of the x_1 oscillation. Throughout ϵ will be kept fixed at 0.1. The equilibrium points of V and their respective energies are listed in Table I.

* Received January 8, 1971.

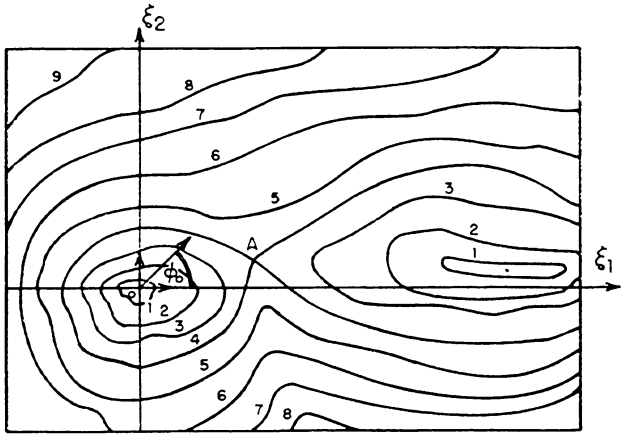

FIG. 1. Contour plot for two bowls.

Note that the model considered has in general three saddle points with the point (b) being invariant in the parameters ν and γ. The saddle point (b) will be henceforth denoted as the "lip" and the energy at the "lip" defined as E_L . Fig. 2 shows a plot of the equipotential energy contours in the $x_1 - x_2$ plane for the indicated values of the parameters.

3. Preliminary Studies. The solution of (2.2) for a particular initial condition and fixed parameters ν and γ lies on a three-dimensional constant-energy manifold of the four-dimensional phase space. The projection of this solution on the x_1-x_2 plane consists of a trajectory which may be of two kinds: (a) the solution trajectory remains confined within the potential well and the solutions $x_1(t)$, $x_2(t)$ describe oscillations whose amplitudes remain bounded, and (b) the trajectory "escapes" from within the well with increasing amplitudes in one or both coordinates. For case (a) the trapped trajectory will generally fill in an "envelope" in the x_1-x_2 plane as, for example, in Fig. 7. In the event that the frequencies of oscillation in the two coordinates are in some integral ratio the "envelope" degenerates to a closed path in the x_1-x_2 plane as in Fig. 13 or Fig. 23.

Preliminary experimental results were obtained by simulating Eqs. (2.2)

TABLE I

Data for equilibrium points of $V(x_1, x_2)$

No.	Coordinates		Potential Energy	Nature
	x_1	x_2		
a	0	0	0	Stable
b	0	$-4/3$	$32/27$	Unstable (saddle)
c	$\bar{x}_1 = \pm\left[\frac{(4\bar{x}_2 + 3\bar{x}_2^2)}{\epsilon\gamma}\right]$	$\bar{x}_2 = \frac{1 - \epsilon\nu}{\epsilon\gamma}$	$2\bar{x}_2^2 + \frac{\bar{x}_1^2}{2} + \bar{x}_2^3 - \frac{\epsilon}{2}(\gamma\bar{x}_1^2\bar{x}_2 + \nu\bar{x}_1^2)$	Unstable (saddle)

on an analog computer. There are some experimental difficulties in determining the exact demarcation between trapped and "escape" solutions. The solution corresponding to the threshold energy level could execute an innumerable number of oscillations before "escape" and this could be influenced by factors such as extraneous phase shifts and dissipative elements in the computer components. Accordingly, a time span corresponding to about 100 cycles of the x_2 oscillation was chosen for ascertaining the nature of the solution.

The first such study was devoted to the determination of the threshold escape energy as a function of the angle ϕ_0 defined by

$$\tan \phi_0 = [\dot{x}_2(0)/\dot{x}_1(0)] . \tag{3.1}$$

Fig. 3 shows the results obtained for selected ν and γ. The variable ϕ_0 is shown only in the interval $-90° \leq \phi_0 \leq 90°$ since the potential energy function is symmetric in x_1. The maximum value of the escape energy occurs for angles close to zero degrees and the loci of the escape energies are not widely different for opposing signs of γ. The locus $\text{cosec}^2 \phi_0$ shows the energy required for escape in the absence of coupling and it is observed that except for $|\phi_0|$ greater than 40° the action of the coupling is to decrease the energy required for escape. Since $-20° < \phi_0 < 20°$ shows the strongest effects of the interesting nonlinear coupling, further studies were made with $\phi_0 = 0$.

Fig. 4 shows the influence of the coupling coefficient γ on the escape energy for $\phi_0 = 0$ and zero detuning. An increased value of $|\gamma|$ leads to an improved energy exchange between the coordinates x_1 and x_2 and, consequently, a lowered value of the escape energy. The experimental data of Fig. 4 are fit quite closely by an empirical formula

$$\frac{E_{\text{escape}}}{E_L} = \frac{1}{1 - \exp - k\,|\gamma|} \tag{3.2}$$

where $k \simeq 0.22$.

For the next set of studies $|\gamma|$ was chosen to be 2 since this was large enough to give a reasonably rapid exchange of energy yet small enough to show a significant increase

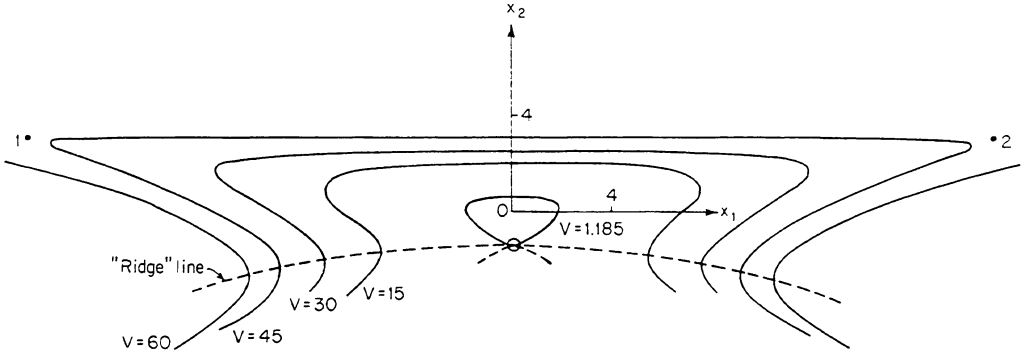

FIG. 2. Equipotential energy contours for $V(x_1, x_2) = 2x_2^2 + 0.3x_1^2 + x_2^3 - .1x_1^2x_2$. ⊗: lip of bowl; 1, 2: two additional saddle points.

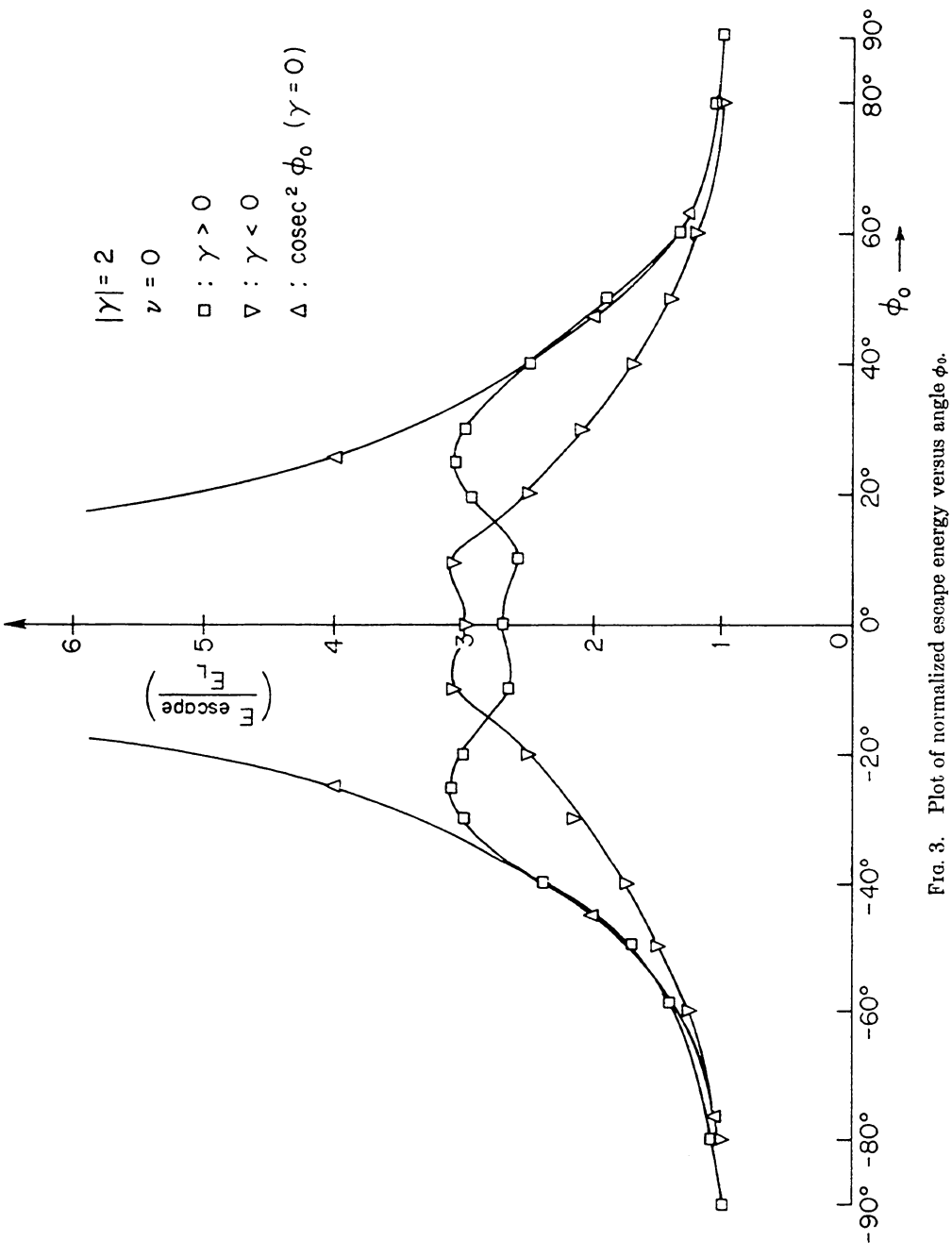

FIG. 3. Plot of normalized escape energy versus angle ϕ_0.

in E_{escape} over E_L . Fig. 5 shows the distribution of the escape energy as a function of ν now for $|\gamma| = 2$ and $\phi_0 = 0$. Curve A (negative γ) shows an approximately linear variation of the escape energy down to a value close to the absolute minimum of 1 (near $\nu = 2$); it is then relatively constant. The x_2^2 term in (2.2b) causes the frequency of an oscillation

confined to this coordinate to decrease as the amplitude is increased. An appreciable energy exchange between the motions x_1 and x_2 can be expected when the frequencies of oscillation in these two coordinates are in a "near resonance" ratio of 1:2. For a large value of the total energy the energy exchange is achieved more completely when ν assumes positive values since this lowers the frequency of the x_1 oscillation and maintains the resonance condition.

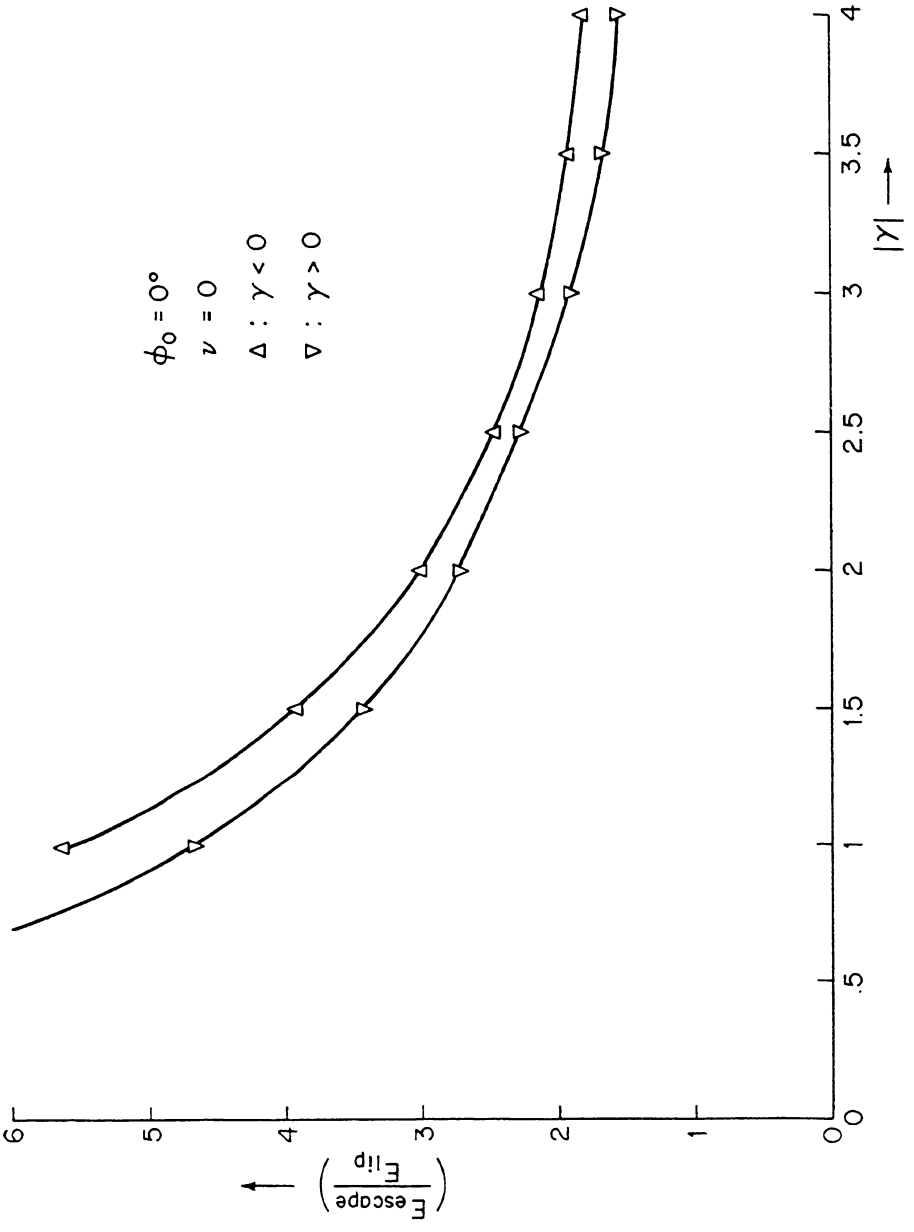

FIG. 4. Plot of normalized escape energy versus coupling coefficient γ.

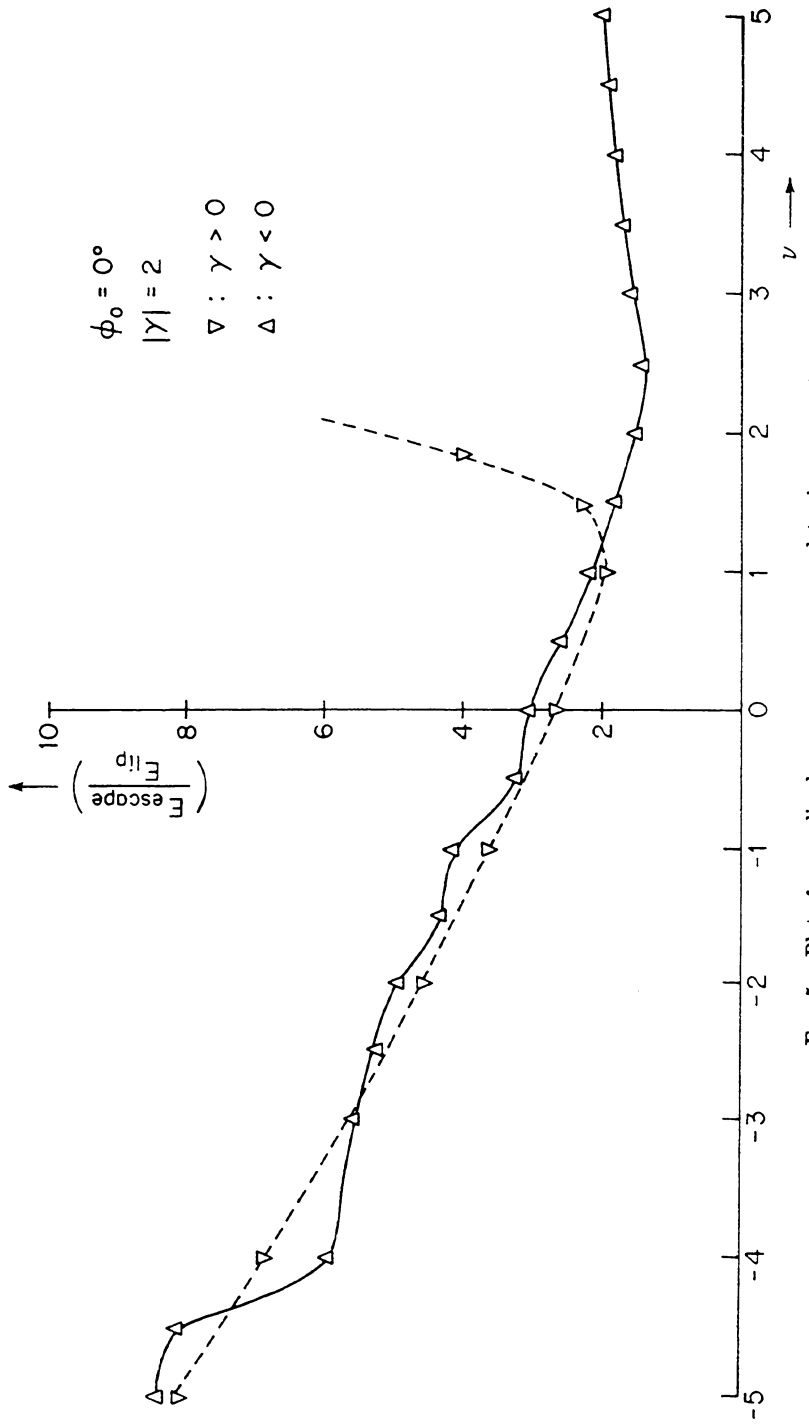

FIG. 5. Plot of normalized escape energy versus detuning parameter ν.

Fig. 5 shows that the results are not widely different for opposite signs of γ so long as ν is negative. For positive γ, however, the escape energy rises steeply when ν takes values greater than 1. This effect is quite striking and indicates the possibility of trapped solutions having energies much in excess of that at the "lip". The subsequent detailed study will be associated with a positive sign for γ.

4.0. Experimental results for positive γ. The results of this study are summarized in Fig. 6, where the vertical axis corresponds to the normalized value of the initial energy E_0 plotted on a logarithmic scale. The only variable initial condition is the velocity for the x_1 coordinate. We will consider now some representative fixed values of ν and describe the kinds of solutions obtained for progressively increasing E_0.

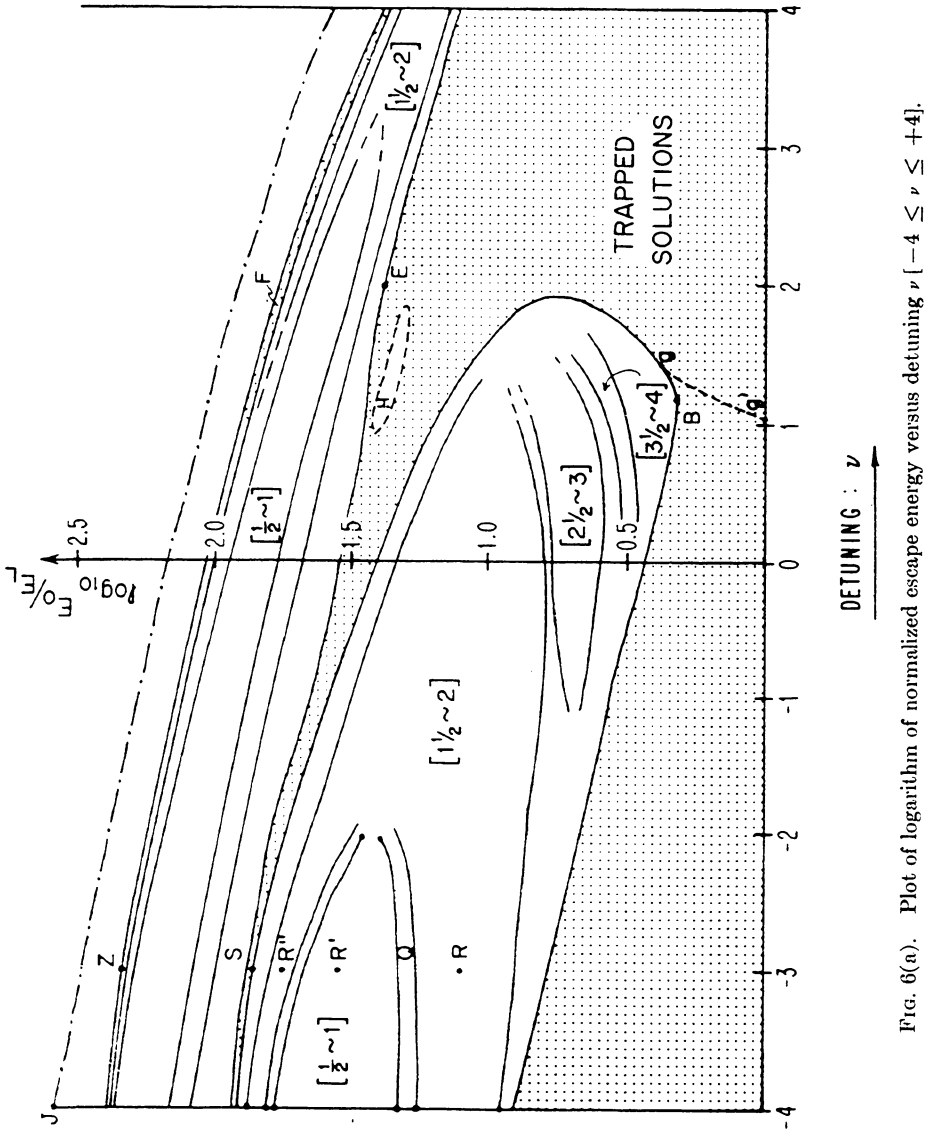

FIG. 6(a). Plot of logarithm of normalized escape energy versus detuning ν [$-4 \leq \nu \leq +4$].

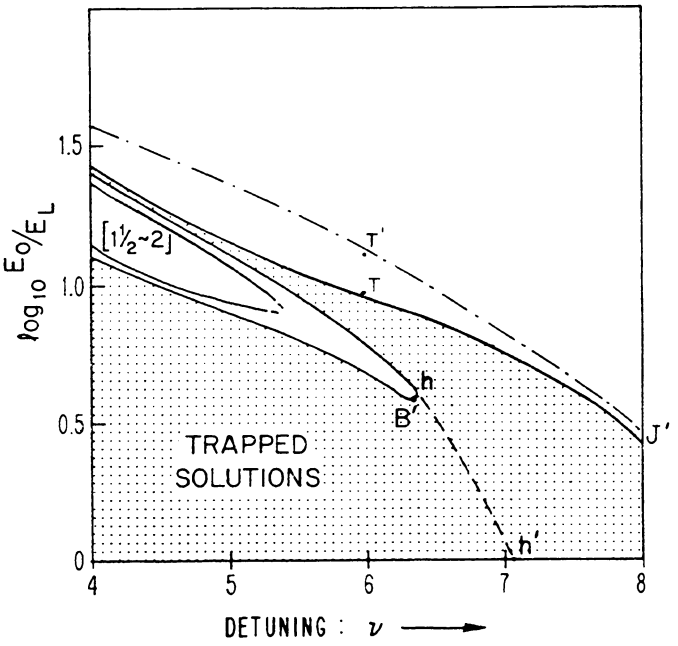

FIG. 6(b). Plot of logarithm of normalized escape energy versus detuning ν [$4 < \nu < 8$].

(a) $\nu = -3$. At low energies the solutions remain trapped and $x_1(t)$ and $x_2(t)$ exhibit slowly varying modulation of the amplitude and phase (see Fig. 7). The first "escape" solution is observed at a value of $\log_{10}(E_0/E_L)$ close to 0.5. Before escape the limiting trajectory makes many oscillations in x_1 and when it finally crosses the potential ridge line it does so at a value of x_1 close to the maximum attained earlier. Repeated runs on the computer for energy levels close to threshold seem to indicate that the envelope "opens" at the sides, as sketched in Fig. 8 for an escape path. It is also observed that prior to "escape" additional "corners" are developed on the side of the envelope away from the "lip". These corners appear to be generated by a subharmonic oscillation of

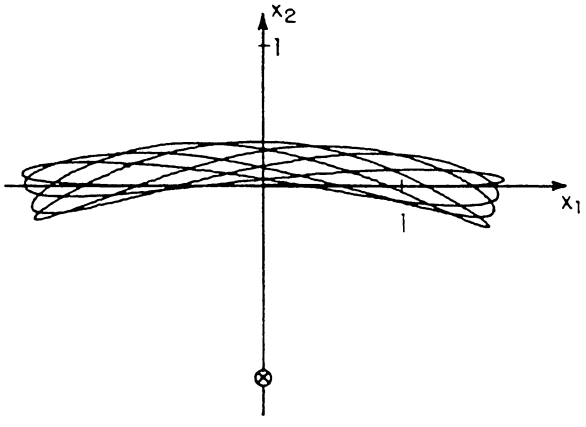

FIG. 7. Trapped solution for an initial x_1 velocity [$\nu = -3$, $\log_{10} E_0/E_L = .228$].

some particular order of the fundamental frequency, primarily in the x_2 coordinate, and it is possible that the escape solution corresponds to unstable growth of this subharmonic component. As E_0 is increased above the threshold the number of oscillations executed prior to escape decreases. The numbers in the square brackets in Fig. 6 indicate the x_2 oscillations before escape. Thus for the energy level R or R'' $1\frac{1}{2}$ to 2 oscillations are observed while at R' $\frac{1}{2}$ to 1 oscillation is found. Curiously, the narrow band containing the point Q has more oscillations (5 to 6) than the regions on either side. There is a strong suggestion that for precisely adjusted initial energy in the vicinity of Q a purely periodic unstable solution may exist (infinite number of oscillations for escape) resembling Fig. 9. As the energy is increased beyond R'' the number of oscillations again increases. Region S is a narrow band of trapped solutions with energies close to 70 times that of the "lip". These solutions exhibit an almost synchronized $x_1 : x_2$ frequency ratio of 1:2. The harmonic content of $x_1(t)$ is predominantly that of the fundamental with a frequency slightly less than 1 radian per second. The solution $x_2(t)$, however, contains a bias term as well as a second harmonic of comparable order to its fundamental. The amplitude in the x_1 coordinate is observed to be about 6 to 7 times that in the x_2 coordinate.

Proceeding to still higher energies, the pattern of behavior repeats. Region Z is another zone where trapping is indicated although this is difficult to establish (6 to 7 trapped cycles have been observed). The x_2 solutions have now acquired a strong third-harmonic component. Above Z only 1 to 2 oscillations are required for escape.

(b) $\nu = 2$. As Fig. 6 shows, there is a continuous band of trapped solutions for energies ranging from zero up to almost 30 times that of the "lip". One important difference between these trapped solutions and those obtained in the low-energy band

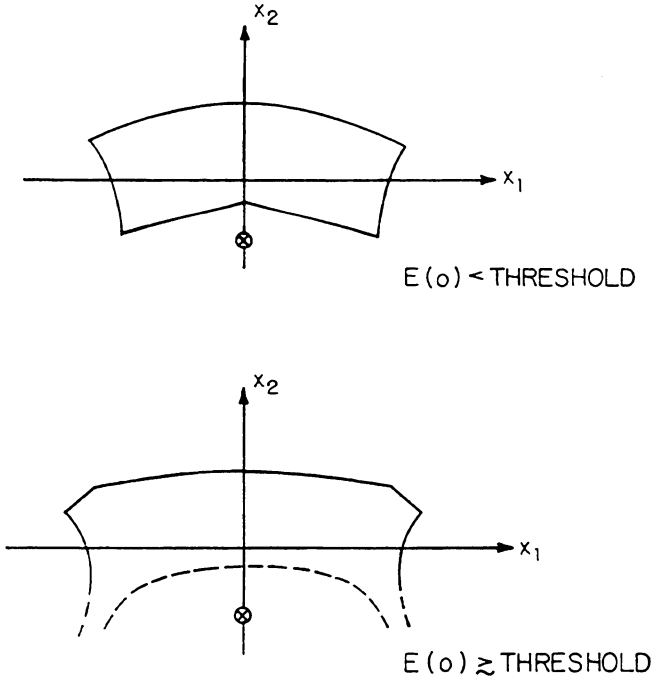

FIG. 8. Possible modification of envelope for an escape trajectory.

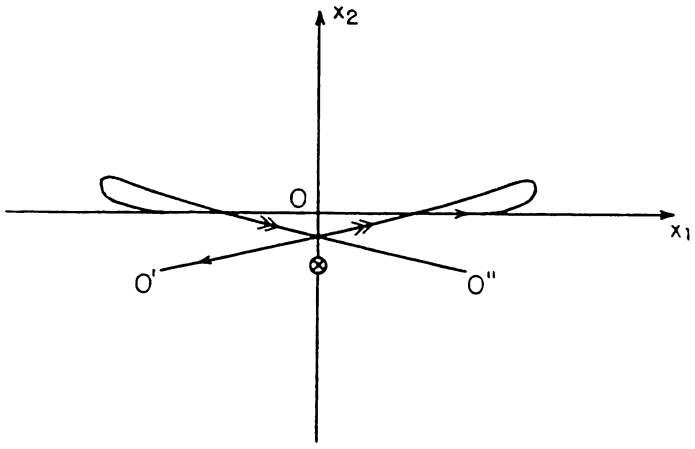

FIG. 9. Possible form of a periodic trajectory in region Q of Fig. 6(a) ($\nu = -3$).

for $\nu = -3$ is in the shape of the "envelope". The envelope for $\nu = 2$ has the general character shown in Fig. 10 (cf. Fig. 7 for $\nu = -3$). The implications of these are discussed in Sec. 4.2. At $\log_{10}(E_0/E_L) \simeq 0.7$, where the "nose" of the region of escape solutions comes close to $\nu = 2$, the rate of modulation of the $x_1(t)$ and $x_2(t)$ trapped solutions as they "fill in" the envelope is quite rapid.

The solutions remain trapped up to E. Region F is another band of trapped solutions which is a continuation of that seen at Z and the solutions have corresponding harmonic content.

(c) $\nu = 6$. For positive ν the linearized x_2 frequency is decreased. It was seen earlier that the lowest point of escape energy (B in Fig. 6) occurred for a value of ν which created "near-resonance" with a frequency ratio of 1:2 in the x_1 and x_2 coordinates. A similar resonance effect with a 1:4 ratio is observed for ν slightly greater than 6.

The band of trapped solutions below T are similar to those seen at Z and F. Above T a new phenomenon is observed. The two high-energy saddles (see Fig. 11) now serve as escape routes despite the fact that their energies are very much greater than the "lip".

Other Details of Fig. 6. The line gg' marks the demarcation between the two different types of envelopes mentioned earlier. Associated with the transition to an increased ν is a noticeable reduction in the energy exchange between x_1 and x_2 . A similar envelope

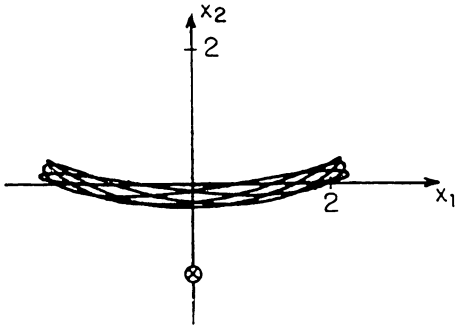

FIG. 10. Trapped solution for initial x_1 velocity [$\nu = 2$, $\log_{10} E_0/E_L = .228$].

transformation is observed for values of ν lying in the neighborhood of hh'. There is, however, very little change in the energy exchange process and the oscillations are confined primarily to the x_1 coordinate.

The region H corresponds to solutions that "escape" after executing at least 5 to 6 oscillations. The significance of this region will be more evident in Sec. 4.4.

The locus JJ' represents the plot of the potential energies at the saddle points (c) obtained from Table I. It is seen that the boundaries separating the regions of trapped and "escape" solutions are almost translates of JJ'. This indicates that although a majority of the solutions "escape" via paths adjacent to the "lip" (the exceptions being seen earlier) the energies of the trapped solutions are roughly proportional fractions of the saddle-point energy obtained from JJ'. The locus JJ' appears to represent an upper bound for the existence of bands of trapped energies.

An examination of Fig. 11 shows that the trajectory undergoes successive "reflections" from the potential energy surface in the neighborhood of the saddle point (c). The form of the tortuous path described leads one to suspect the existence of a large number of bands of trapped solutions, the band width diminishing rapidly with increasing energy levels. The interval TT' in Fig. 6b could, for example, contain very narrow bands of such trapped solutions.

4.1. Related periodic solutions. An examination of the trapped solutions, particularly those where the envelope is narrow, discloses that the motion can be decomposed into a small variation about a large strictly periodic motion. The solutions which ultimately escape have a similar behavior during their pre-escape phase. This suggests that the question of escape can be related to the stability of an associated periodic solution of equal energy. To pursue this line of study it is first necessary to find the periodic solutions and this requires an extension of the initial condition range. Since the envelopes considered here are symmetric about $x_1 = 0$ in the x_1-x_2 plane, only corresponding symmetric periodic solutions will be sought. Appropriate initial conditions are $x_1(0) = 0$; $\dot{x}_2(0) = 0$ while $\dot{x}_1(0)$, $x_2(0)$ are in general nonzero.

Fig. 12 shows the initial conditions that correspond to periodic solutions. For a given ν they are seen to be on continuous loci in the $\dot{x}_1(0)$, $x_2(0)$ plane. There are several separate loci for each ν and, considering ν to be a parameter, the loci can be grouped into related "families". Marked on each locus are the regions of trapped and escape solutions. That is, in the "escape" region any small iso-energetic displacement in the four-dimensional phase space from the periodic solution will generate an escape trajectory. (Clearly a displacement to a neighboring periodic solution of different energy will remain trapped.)

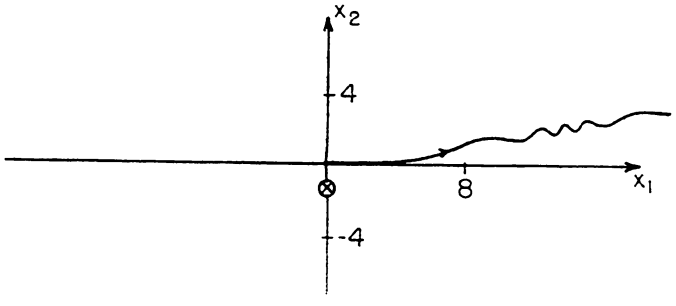

FIG. 11. Escape path for an initial x_1 velocity [$\nu = 6$, $\log_{10} E_0/E_L = 1.152$].

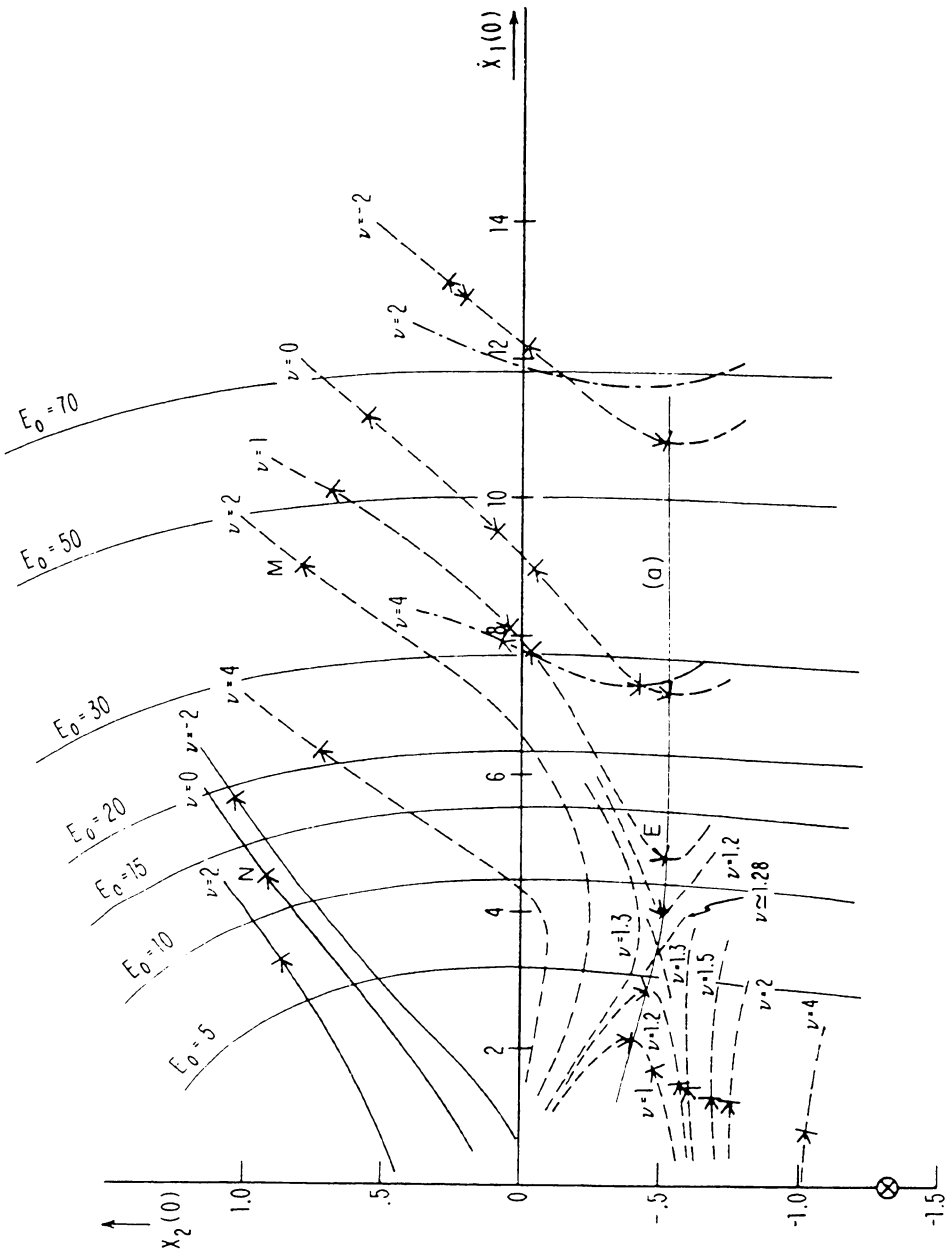

FIG. 12. Plot of family of periodic solutions for different values of detuning ν. ⊗: position of "lip"; ———: Family #1; - - - - -: Family #2; —·—·—: Family #3; ——→|: Limit of trapped solution; (a): Locus of vertical tangents to Family 2 solutions.

For the "trapped" regions of the loci a sufficiently small displacement from the periodic trajectory will remain trapped.

Note that the distinction "trapped" and "escape" does not correspond directly with stability in the Lyapunov sense. Linearized variational equations can be written for any

periodic solution and stability determined from a set of coupled Hill's equations (see Sec. 5.1). This determination of stability is Lyapunov, although the conservative nature of the system gives stability only in the neutral sense. A periodic solution may meet the definition "trapped" and yet be linearly unstable. This is because the effect of nonlinearities in the variational equation is to limit the extent of the disturbance growth. An "escape" periodic solution is necessarily linearly unstable. Since the results of Fig. 12 are determined by computer studies, linearly unstable periodic solutions are difficult to locate, and those for which escape occurs are especially difficult.

4.2. Character of periodic solutions and their instabilities. *Family No.* 1. Fig. 13 shows an example of a trapped periodic motion for $\nu = 0$. An examination of the x_1 and x_2 time plots shows each motion to be predominantly simple harmonic. The period of oscillation decreases slightly from the linearized value for increasing energies. For energies exceeding N (see Fig. 12) the solutions "escape" (e.g. Fig. 14) and the number of cycles executed prior to escape decreases with increasing energy. Trapped periodic solutions on the locus $\nu < 0$ can be continued to a higher energy level than those for $\nu > 0$. Further the solutions for $\nu < 0$ seem to approach the origin asymptotically in contrast to those for $\nu > 0$ which appear to originate at some finite coordinate on the $x_2(0)$ axis.

The trapped solutions described in Sec. 4.0 were generated for $x_2(0) = 0$. That is, they correspond to points on the horizontal axis in Fig. 12. Therefore the periodic solution appropriate to the trapped motion is the one which is closest to that axis at a given energy level. Thus for $\nu = 0$, for all $\dot{x}_1(0)$ up to about 6, it is clearly the first family of periodic solutions which is relevant, while in the neighborhood of $\dot{x}_1(0) = 9$ it is the second family. However for $\nu = 2$ the second family is the relevant one from $\dot{x}_1(0) = 0$ up to about 9 or 10. Referring now to Fig. 6a, the line gg' dividing the low energy trapped solutions into two groups near $\nu = 1$ represents the demarcation between Family 1 and Family 2 as the relevant periodic solution. Of course this distinction is not a really sharp one. For clarity the loci $\nu = 6$ and 8 have not been shown in Fig. 12, yet it can be remarked that the dividing line hh' in Fig. 6b corresponds to a transition from Family 2 to Family 3 as the relevant periodic solution for large detuning.

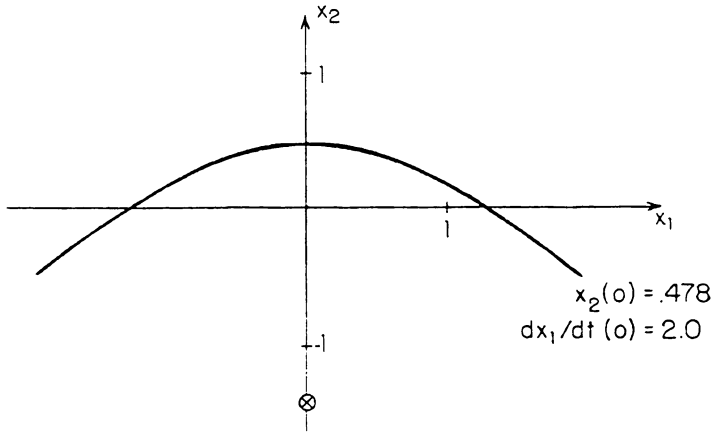

FIG. 13. Stable periodic solution (Family 1).

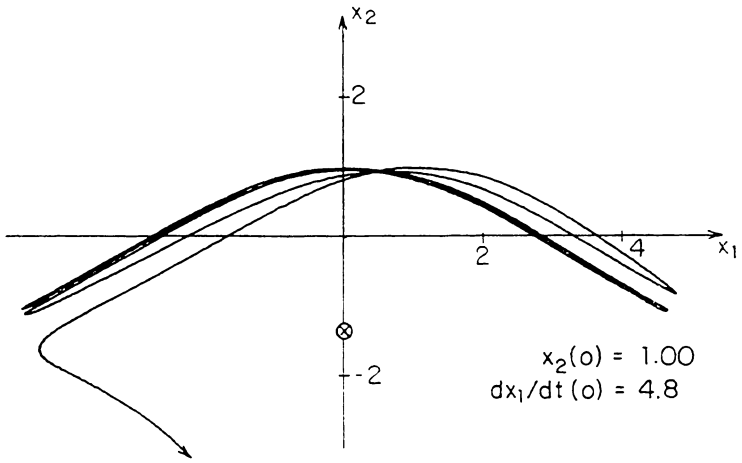

FIG. 14. Unstable periodic solution (Family 1) ($\nu = 0$).

Family No. 2. For $\nu = 2$, there is one locus that starts near the origin, intersects the $\dot{x}_1(0)$ axis at about 6.5 and solutions remain trapped up to M (Fig. 12). Figs. 15 and 16 show two examples of periodic motions along this locus. In contrast to Family No. 1 the $x_2(t)$ solution now has a prominent bias term as well as a double frequency component. The harmonic component of $x_1(t)$ remains predominantly that of its fundamental. The period of oscillation is found to increase slightly with increasing energies. Note that there are two branches of the loci although the second has been determined only for $\nu > 1$.

Fig. 12 also shows the presence of a "saddle" for a value of ν near 1.2. A stability analysis (Sec. 5.2) will show the locus of vertical tangents to be the bounds of linearized stability. Note that there are solutions below the vertical tangent that are stabilized nonlinearly. These are essentially due to energies being less than the "lip" with slight extensions for some values of ν.

The high-energy branches of Family No. 2 have generally a threshold of escape for $x_2(0) \simeq -0.5$ corresponding roughly to the locus of vertical tangents. These branches also have an escape threshold for $x_2(0) \simeq 0.5$. In between, near $x_2(0) = 0$, there is a "wedge" of escape solutions starting approximately at $\nu = 1.5$ and growing in width as ν decreases. The linear instability associated with these "escape" solutions shows a strong $\frac{1}{2}$ subharmonic content along with 3/2 and 5/2 components. For $\nu = 2$ where the motion is not actually unstable (no "escape"), the disturbances from the periodic motion have the same strong subharmonic modulation. From the $\nu = 4$ and $\nu = 6$ curves of Family No. 2 it might be expected that a broad band of trapped motions would persist for large ν down to $\dot{x}_1(0) = 0$. In fact this is not the case. For $\nu = 10$, the remote saddle points in the potential energy (Fig. 2) have moved into the origin and the origin itself becomes a saddle-type singularity. Thus as ν increases from 6 up to 10 the upper bound of the trapped solutions in Fig. 12 comes down toward the origin.

Family No. 3. The interval of trapped motions is quite narrow and diminishes rapidly with decreasing ν. The solutions $x_1(t)$ and $x_2(t)$ now have additional third-harmonic components. For $\nu < 2$, subharmonic components (primarily of order $\frac{1}{2}$) are observed to be so readily generated for very small displacements that it is almost impossible to isolate the main periodic solution on the computer.

4.3. Periodic solutions with longer periods (subharmonic components). In the previous section we have remarked on the occurrence of strong subharmonic content for trajectories in phase space that are slightly displaced from the pure periodic motions. Different orders of subharmonics occur at different locations on the loci of periodic solutions and the subharmonic of order $\frac{1}{2}$ is especially significant, being associated with linearized instability and "escape" from the well. This suggests that a study of periodic motions with periods of multiples of that of the basic motion would be relevant to the "escape" problem.

Consider linearized perturbations η_1 , η_2 from a basic periodic motion $x_1(t) = x_1^*(t)$ and $x_2(t) = x_2^*(t)$ respectively. The frequencies of oscillation in $x_1^*(t)$ and $x_2^*(t)$ are ω_1 and ω_2 which are in a ratio of 1:2, with the composite system period close to 2π. The variational equations are reciprocally coupled through Mathieu-type terms. If we postulate the lowest rational subharmonic frequency in η_2 to be $\sigma_2\omega_2$, then the Mathieu terms in the η_2 are found to generate the complementary subharmonic $(1 - \sigma_2)\omega_2$. Thus the only range of σ_2 to be considered is $0 < \sigma_2 \leq \frac{1}{2}$. Next, if we examine the effect of the $\sigma_2\omega_2$ component via the Mathieu terms in the η_1 equations, the lowest component in the η_1 has the frequency $\sigma_1\omega_1$ with $\sigma_1 = 1 - 2\sigma_2$. Finally, the effect of the $\sigma_1\omega_1$ component of η_1 in the η_2 equation yields the same $\sigma_2\omega_2$ with which we began. Thus the relation $\sigma_1 + 2\sigma_2 = 1$ links the lowest-frequency component in η_1 and η_2 for any consistent solution of the linearized variational equations. Note that for $\sigma_1 = \sigma_2 = \frac{1}{3}$ the order of the subharmonic is the same for both x_1 and x_2, while for $\sigma_2 < \frac{1}{3}$, x_2 has the lowest-order subharmonic and for $\sigma_2 > \frac{1}{3}$, x_1 has the lowest-order. In no case is the lowest order of the composite set $\{\sigma_1 , \sigma_2\}$ greater than $\frac{1}{3}$. Figs. 17 and 18 show loci of initial conditions leading to subharmonic periodic motions for $\nu = 2$ and $\nu = 0$ respectively. These loci bifurcate from the main "stem" locus of Families 1 and 2. The captions ($\frac{1}{2}$, $\frac{1}{3}$ etc.) denote the value of σ_2 . The periodic motions contain strong components at multiples of the lowest frequency and it is especially important to note that the strongest component in x_2 is $(1 - \sigma_2)\omega_2$ rather than $\sigma_2\omega_2$ itself.

Interesting characteristics of these periodic subharmonic motions for $\sigma_2 < \frac{1}{2}$ can be discovered by studying the representative case $\sigma_2 = \frac{1}{3}$ in some detail. The x_1-x_2 trajectory is shown in Fig. 19. The period of this motion is $6\pi/\omega_1$ or $12\pi/\omega_2$. Any point on this trajectory can be regarded as a set of initial conditions, and in particular if we restrict ourselves to crossing of the x_2 axis in the positive x_1 direction we generate three sets of initial conditions for the trajectory which are displayed as the points k, k' and k'' in

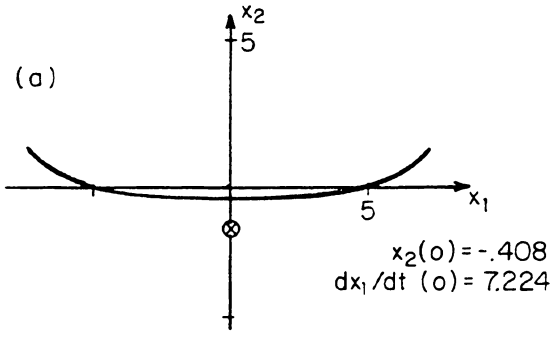

FIG. 15. Nature of periodic solutions for Family 2 ($\nu = 0$).

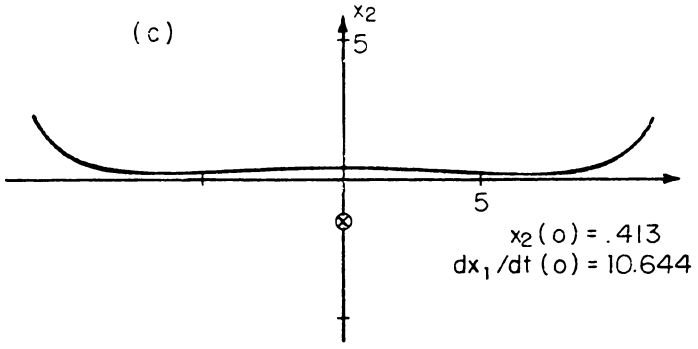

FIG. 16. Nature of periodic solutions for Family 2 ($\nu = 0$).

Fig. 20. The actual execution of the trajectory is a succession of transitions $k \rightarrow k' \rightarrow k'' \rightarrow k$, etc. In the initial condition space of Fig. 20 there is actually a continuum (two-dimensional surface) of points which correspond to periodic solutions and which are associated in sets of three. This is indicated in the figure. Iso-energy contours on this surface of periodic solutions are roughly elliptical. For initial conditions lying just off the surface the motion of the system is almost periodic, and in terms of x_2 axis crossing, successive points in the space of Fig. 20 follow approximately the k, k', k'' transitions

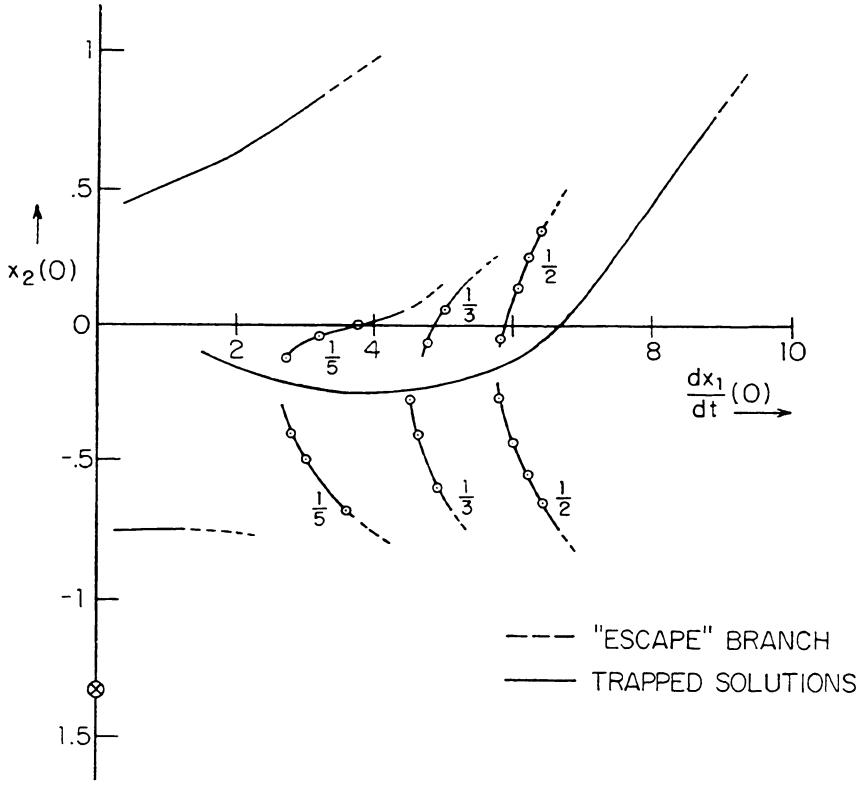

FIG. 17. Family of periodic solutions with subharmonic components ($\nu = 2$).

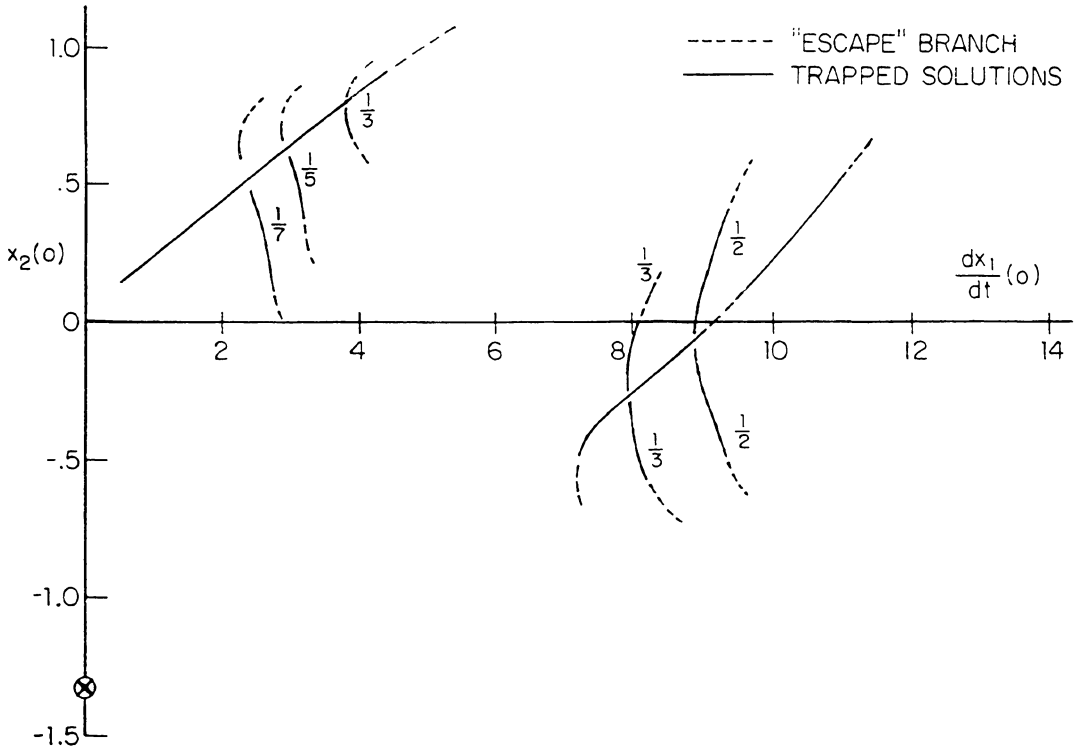

FIG. 18. Family of periodic solutions with subharmonic components ($\nu = 0$).

except that there is a slow, progressive displacement of each point along the iso-energy contour. The x_1-x_2 trajectory corresponding to this slow displacement is shown in Fig. 21, where it is seen that the trajectory slowly fills an envelope.

The existence of a surface of subharmonic periodic solutions is characteristic of all $\sigma_2 < \frac{1}{2}$ and can be interpreted as phase independence of the subharmonic components with respect to the generating solution. For $\sigma_2 = \frac{1}{2}$ the situation is very different. Periodic solutions exist only on two lines in the initial condition space (Fig. 22). One of the lines

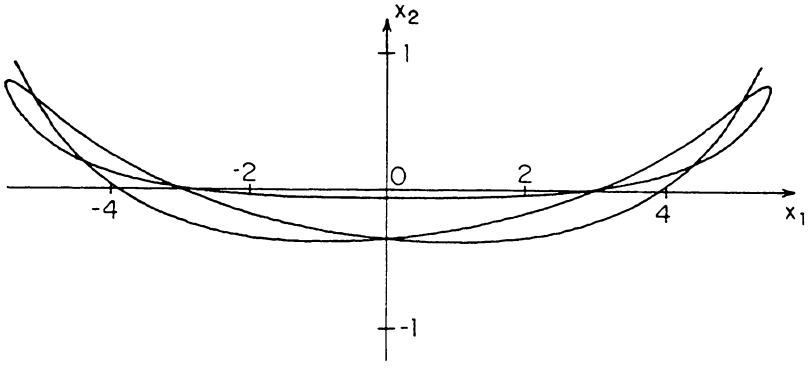

FIG. 19. Trajectory corresponding to periodic subharmonic motion for $\sigma_2 = 1/3$ ($\nu = 2$; $x_2(0) = -0.06$, $\dot{x}_1(0) = 4.644$).

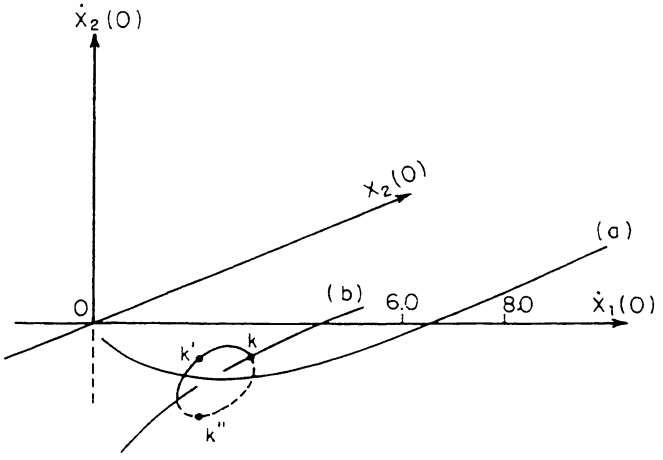

FIG. 20. Initial conditions in 3-space for generating subharmonic motion of order 1/3. ($\nu = 2$). k, k', k''-Equivalent sets of intial conditions generating trajectory shown in Fig. 19; (a) main periodic solution (Family 2) (no subharmonics); (b) symmetric subharmonic loci (lies in $x_2(0) - \dot{x}_1(0)$ plane).

corresponds to symmetrical solutions in the x_1-x_2 plane (Fig. 23), while the other corresponds to asymmetrical solutions (Fig. 24). The two lines appear to join the locus of regular periodic solutions (i.e. nonsubharmonic) at the same point for $\nu = 2$. For $\nu = 0$, however, the bifurcation of the asymmetric branches from the main "stem" occurs at a slightly higher energy level than that corresponding to the symmetric branches. Considering a family of constant-energy surfaces there would exist one critical surface which is tangential to the bifurcation point of the symmetric periodic solutions. For energy levels greater than this critical, there are in general four points of intersection (in pairs of two) with the symmetric and asymmetric branches. Considering the symmetric branch, for a precisely adjusted initial condition (e.g. p or p' in Fig. 22), unlike the other values of σ_2 discussed earlier, there arises no transition sequence from p or p'. For small displacements away from the exact conditions necessary for periodic motions there are slow motions in orbits surrounding p or p'. The asymmetric branches exhibit an unstable characteristic and for $\nu = 0$, small displacements from the branch escape. For $\nu = 2$,

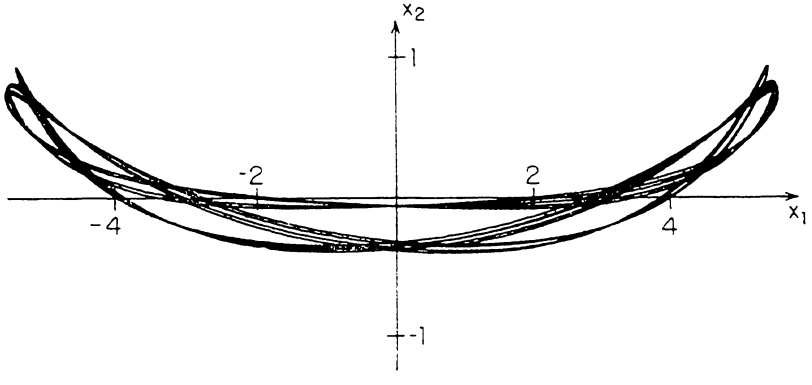

FIG. 21. Trajectory corresponding to an almost periodic motion ($\nu = 2$; $x_2(0) = -.06$, $\dot{x}_1(0) = 4.660$).

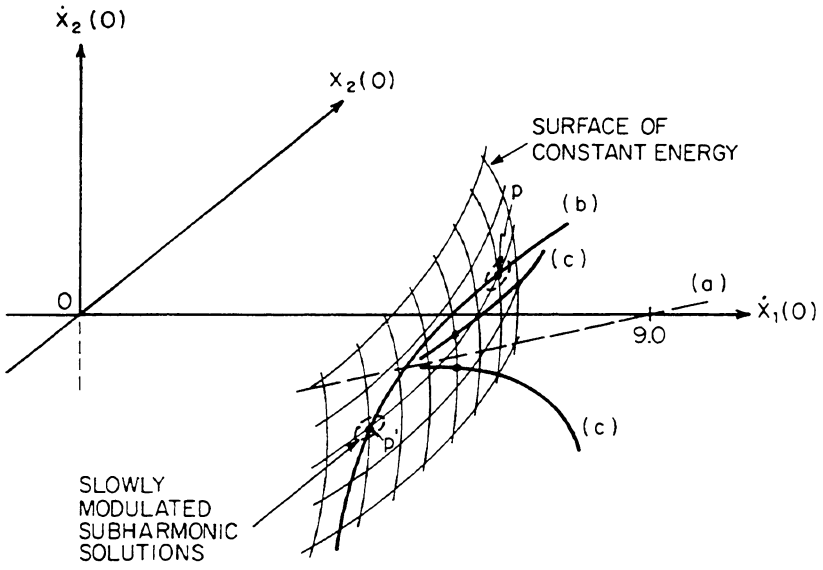

FIG. 22. Symmetric and asymmetric subharmonic loci for order $1/2(\nu = 2)$. (a) main periodic oscillation (Family 2) no subharmonics; (b) symmetric subharmonic loci (lies in $\dot{x}_1(0), x_2(0)$ plane); (c) a symmetric subharmonic loci (lies in space, $\dot{x}_1(0), x_2(0), \dot{x}_2(0)$).

not all such solutions escape and there is a small interval of energies near the bifurcation point where there are amplitude-modulated trapped motions. The theory to be discussed in Sec. 5.1 shows that a periodic motion $x_1(t) = x_1^*(t); x_2(t) = x_2^*(t)$ having a fundamental period T can exhibit linear instability under two conditions:

(1) The characteristic exponent of the system of Hill's equations has a zero exponent.

(2) The exponent has an imaginary part of π/T.

Note that the above are only necessary and not sufficient conditions. Condition (2) corresponds to the generation of a subharmonic component of order $\frac{1}{2}$ and for $\nu = 0$ we notice "escape" for both Families No. 1 and 2 (Fig. 12) near the $\frac{1}{2}$ subharmonic bifurcation point. The Family No. 1 instability is very pronounced and the $\frac{1}{2}$ subharmonic

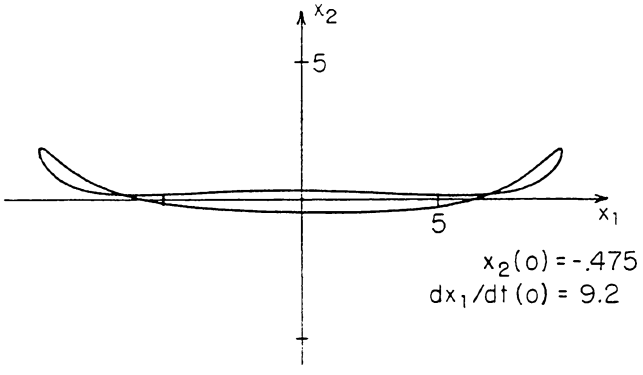

FIG. 23. Nature of solution in presence of a subharmonic component of $\sigma_2 = 1/2\,(\nu = 0)$.

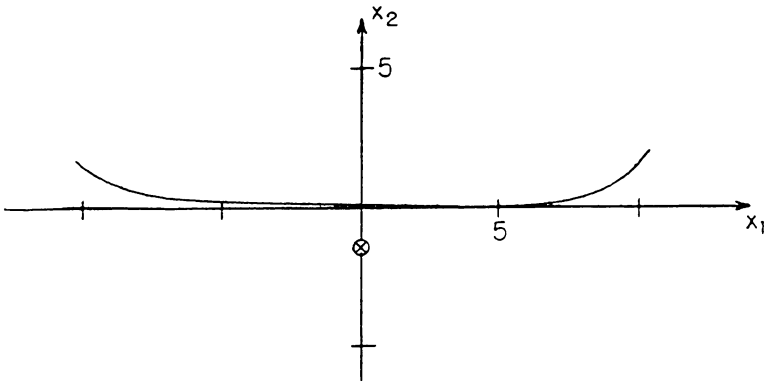

FIG. 24. Trajectory corresponding to an asymmetric subharmonic motion for $\sigma_2 = 1/2$ ($\nu = 0$; $x_2(0) = .05$, $\dot{x}_1(0) = 9.53$ $\dot{x}_2(0) = -.316$).

branch could not even be located. For $\nu = 2$ the $\frac{1}{2}$ subharmonic branch is equally difficult to detect for Family No. 1, whereas for Family No. 2 strong subharmonic modulations are observed near the bifurcation point with the solutions remaining trapped. It has been observed that the transition from a stable to an "escape" behavior along the $\frac{1}{2}$ subharmonic branches of Figs. 17 and 18 is again characterized by condition (2)—that is, the growing motion has a $\frac{1}{2}$ subharmonic of the $\frac{1}{2}$ subharmonic.

4.4 Regions of trapped solutions in the $x_2(0) - \dot{x}_1(0)$ plane ($\dot{x}_2(0) = x_1(0) = 0$). Figs. 25 through 29 show the regions of trapped solutions for the indicated values of the detuning parameter ν. The boundaries were obtained by a computer search facilitated by the stability limits of Families 1, 2, 3 and the subharmonic branches described in the previous section. Also drawn on the figures are the loci of constant total energy $E_0 = 2x_2(0)^2 + x_2(0)^3 + \dot{x}_1(0)^2/2$.

Figs. 25 and 26 show the presence of a wide band of trapped solutions neighboring the origin. The boundary of this region is comprised of a finger-like extension whose "backbone" is the locus of Family No. 2 solutions. Other extensions are caused by Family No. 1 solutions and the $\frac{1}{2}$ subharmonic component locus of Family No. 2. For $\nu = 2$ (Fig. 26) the upper boundary of the regime of trapped solutions comes close to the $\dot{x}_1(0)$ axis for E_0 in the range of 5 to 10. This corresponds to the proximity of the "nose" of the escape solutions to the $\nu = 2$ axis in Fig. 6. For $\nu = 4$, a second narrow region of trapped solutions is found for $E_0 \simeq 26$ and this corresponds to solutions neighboring Family No. 3. There must be a similar region for $\nu = 2$ at $E_0 \simeq 65$ and lying near the horizontal axis. It has, however, not been shown on account of the uncertainty of the long-time containment of these solutions.

For $\nu = 1$ (Fig. 27) there exist three separate regions of trapped solutions. The narrow band of escape solutions near $\dot{x}_1(0) = 8$ corresponds to the region H shown in Fig. 6. For decreased ν (Figs. 28, 29) the regions of trapped solutions are wider apart with a narrowing of the high-energy solutions neighboring Family No. 2. For $\nu = -2$ (Fig. 29) there exist only two trapped regimes separated by a wide band of escape solutions.

On the basis of the above figures it can be expected that for $\nu < -2$ the triangular high-energy trapped region would become narrower whereas the trapped solutions neighboring Family No. 1 would be extended to higher energies. Note that the positive

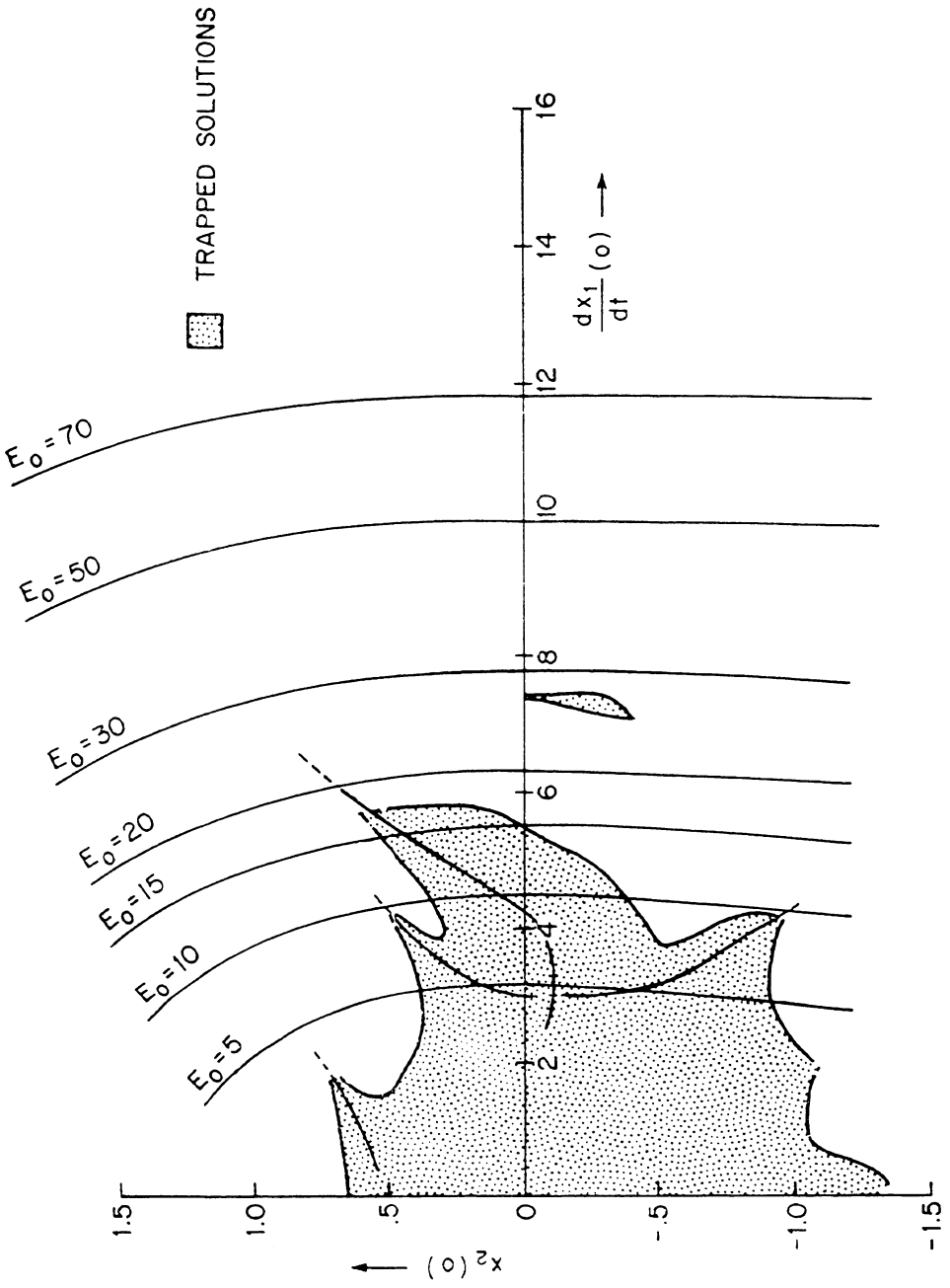

FIG. 25. Region of trapped solutions for $\nu = +4$.

intercept of the trapped solutions (Figs. 25 through 29) on the $x_2(0)$ axis is always 0.67 and corresponds to the energy at the "lip".

5.0. Analytical study. The analysis described below is essentially a stability study for the families of periodic motions, and is divided into two sections. In Sec. 5.1 we consider the linearized variational equations. These coupled Hill's equations are especially

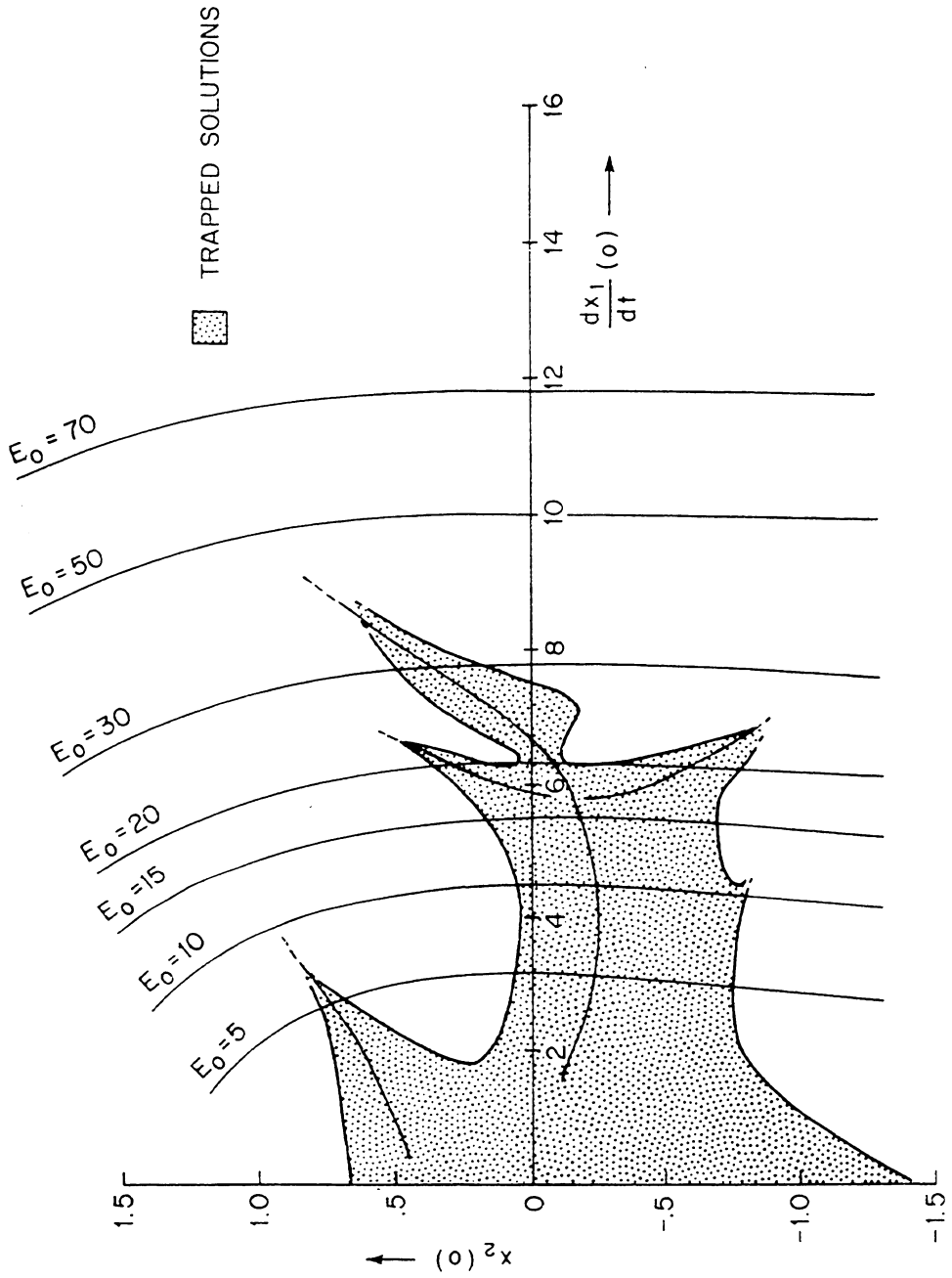

FIG. 26. Region of trapped solutions for $\nu = 2$.

well suited to certain high-energy cases where there are rapid modulations of the solutions neighboring the periodic motion. In Sec. 5.2 we adopt the technique of slowly varying amplitude and phase. This technique is generally applicable only to low-energy cases, but in these cases it permits a more complete description of modulated solutions than the linearized variational equations.

5.1. Stability analysis using Hill's equation. For a general two-degree-of-freedom conservative system possessing the energy integral $U = (\dot{x}_1^2 + \dot{x}_2^2/2) + V(x_1, x_2)$ where $V(x_1, x_2)$ is the potential energy, the equations of motion are

$$\ddot{x}_i + V_{x_i} = 0, \qquad i = 1, 2. \tag{5.1}$$

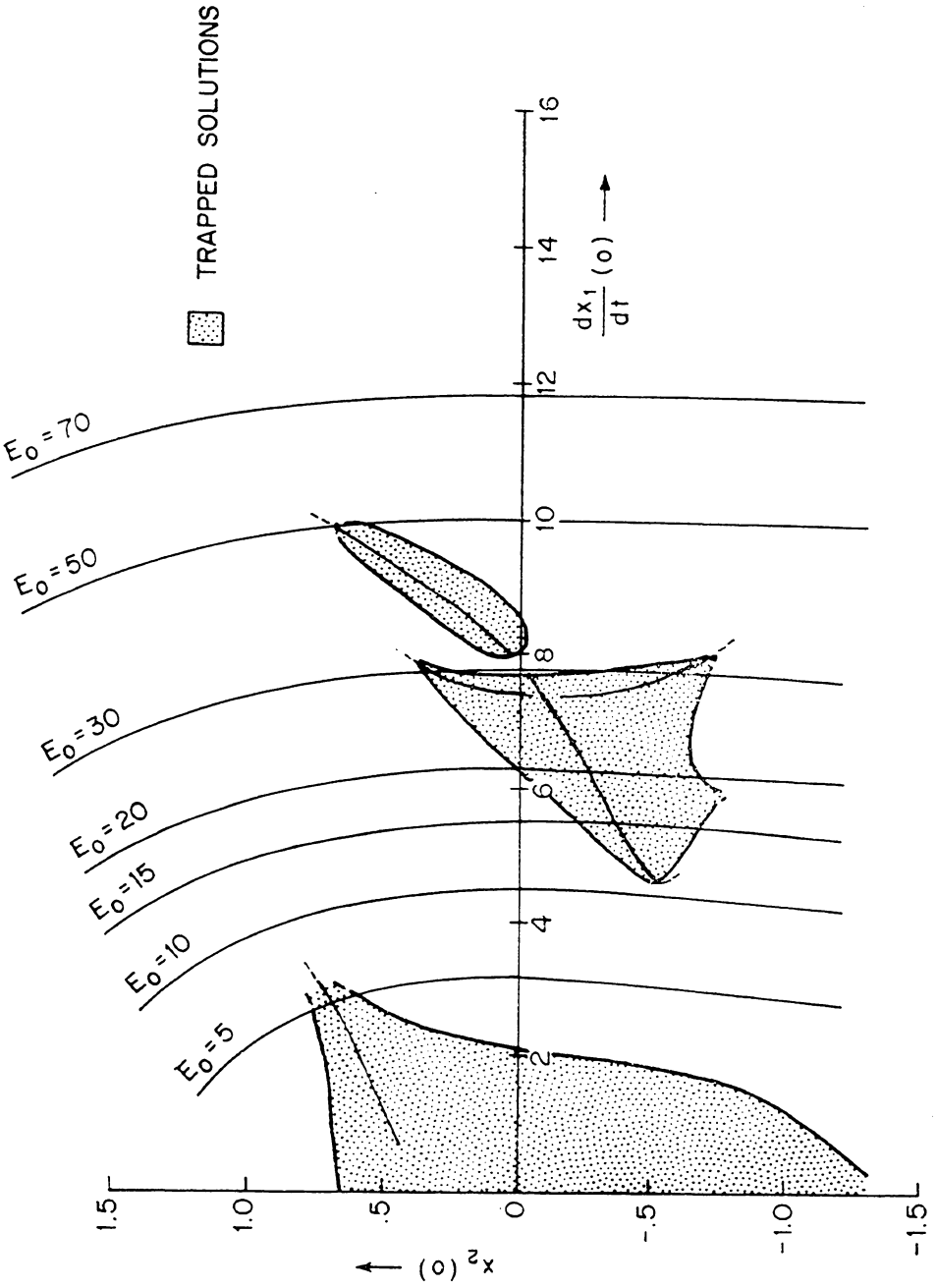

FIG. 27. Region of trapped solutions for $\nu = 1$.

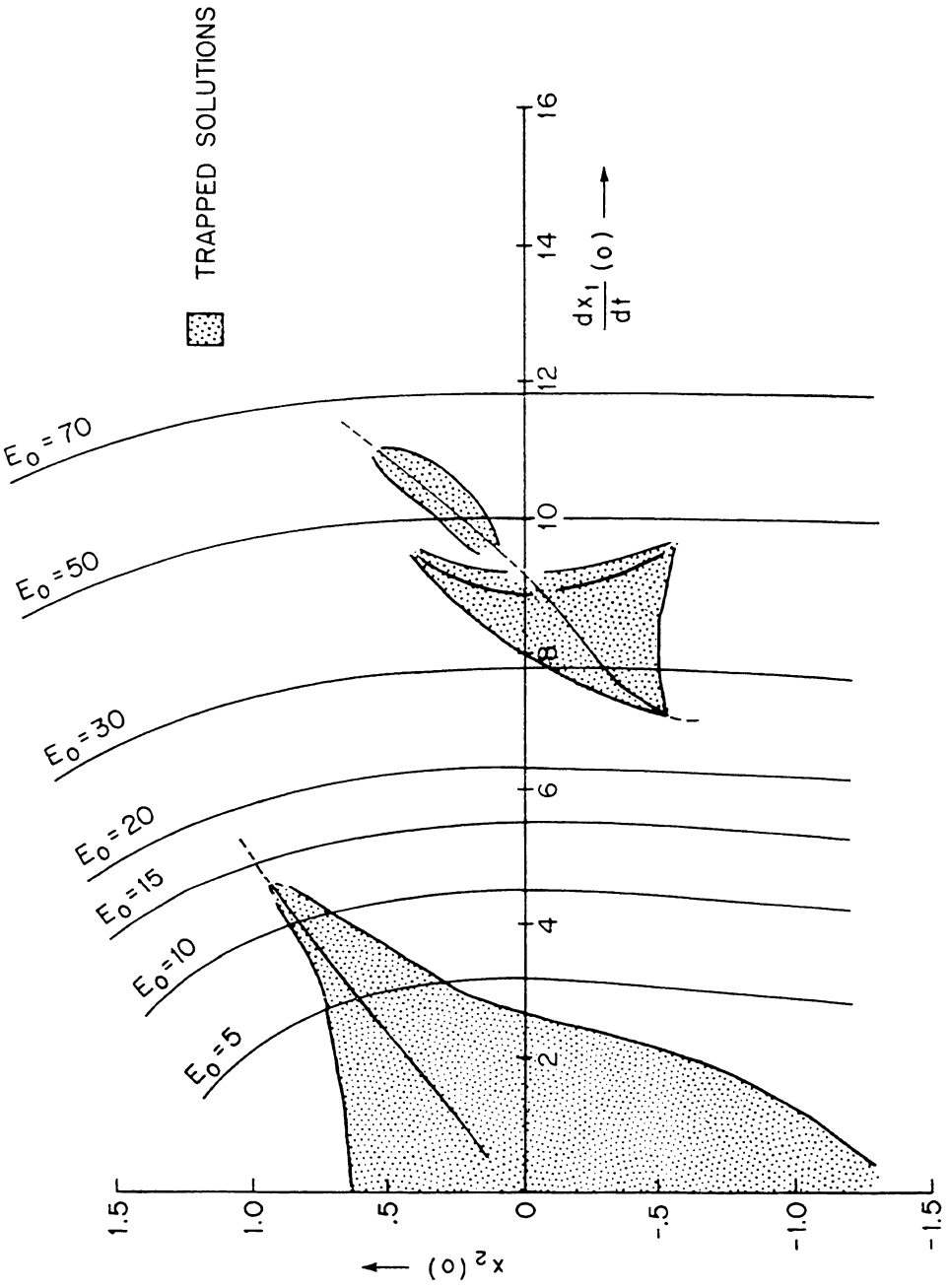

FIG. 28. Region of trapped solutions for $\nu = 0$.

If we assume a periodic motion $x_1^*(t)$, $x_2^*(t)$ with a least common period T, the linearized variational equations are

$$\ddot{\eta}_i + \eta_i V_{x_i x_i} + \eta_{3-i} V_{x_i x_{3-i}} = 0, \qquad i = 1, 2 \tag{5.2}$$

where the η_i are perturbations around the periodic motions x_1^* , x_2^* and the partial derivatives of $V(x_1 , x_2)$ are evaluated for the assumed periodic motion.

The system of equations (5.2) admit the well-known Floquet theory with the general solution

$$\eta_i = \sum_{i=1}^{4} c_i e^{\alpha_i t} p_{ii}(t), \tag{5.3}$$

where the c_i are integration constants, α_i the characteristic exponents, and the $p_{ii}(t)$

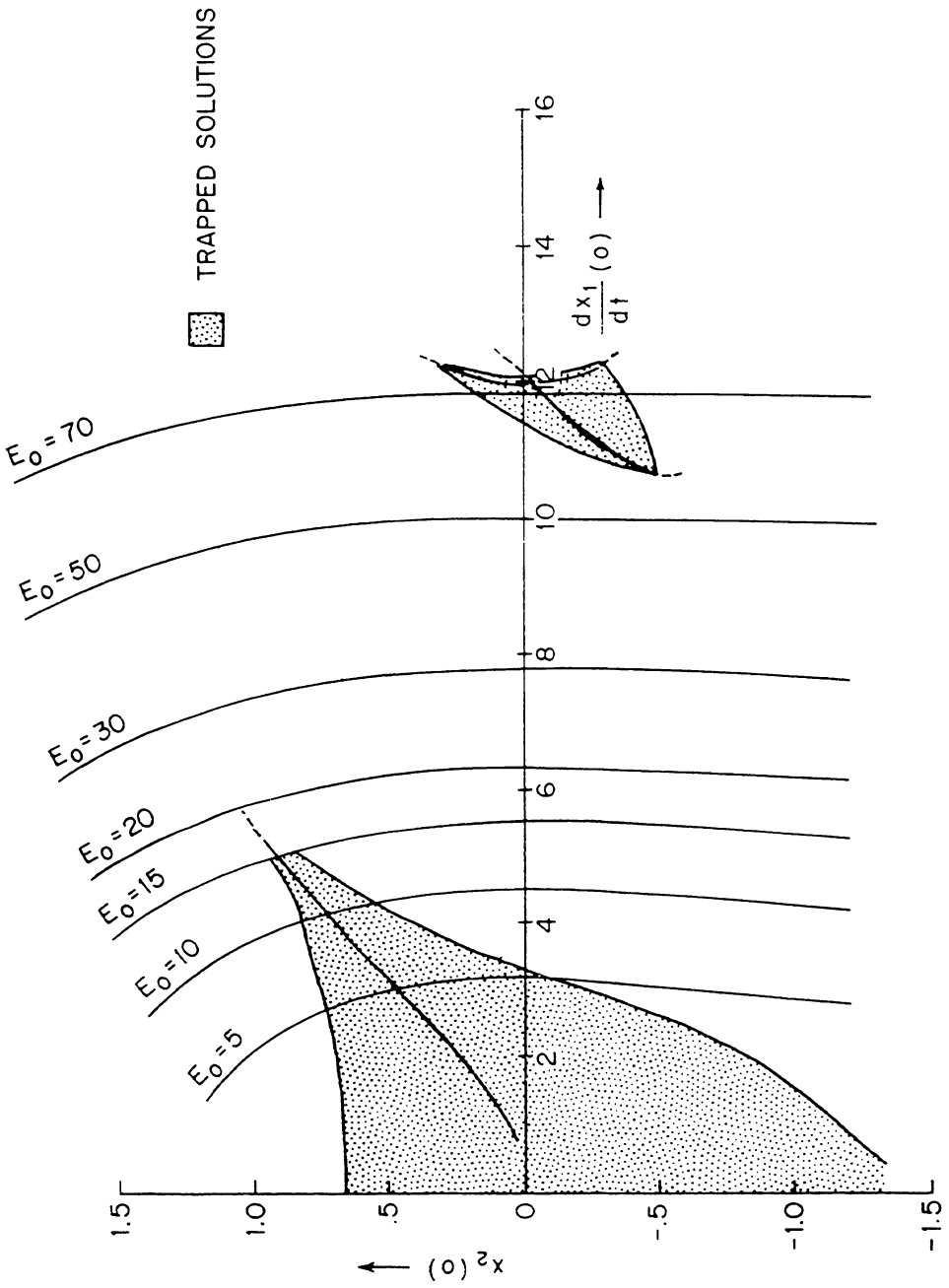

FIG. 29. Region of trapped solutions for $\nu = -2$.

periodic functions with period T. The autonomous equations of motion (5.1) can be expressed in a canonical form and Poincaré [6] has shown that in such cases the characteristic exponents are equal in pairs but with opposite signs. Two of these exponents are always zero and they correspond respectively to perturbations that (1) shift by a constant factor the argument of time of the periodic motion $x_1 = x_1^*(t)$; $x_2 = x_2^*(t)$; (2) displace the motion to a neighboring periodic motion at a slightly different energy level and period. The other two exponents $(\alpha, -\alpha)$ are in general nonzero and serve to determine the stability. A necessary condition for stability is that α be purely imaginary. As a consequence of the two zero exponents the characteristic equation determining α is similar to that obtained for a single-degree-of-freedom system and in particular linear instability is found when α is equal to zero or $i\pi/T$. When $\alpha = 0$, all four exponents vanish and the stable variational solution has a period T. When $\alpha = i\pi/T$ the variational solution has a modulation frequency $\frac{1}{2}$ of the basic frequency of the unperturbed periodic motion.

The variational equations (5.2) for the particular problem considered here can be written as a pair of coupled Hill's equations:

$$\ddot{\eta}_1 + [1 - 0.1\nu - 0.2x_2^*(t)]\eta_1 = 0.2x_1^*(t)\eta_2 , \tag{5.4}$$

$$\ddot{\eta}_2 + [4 + 6x_2^*(t)]\eta_2 = 0.2x_1^*(t)\eta_1 . \tag{5.5}$$

For many cases of interest the computer tests reveal that when instability is seen the variations η_2 are much stronger than η_1 . This suggests an approximate analysis which ignores the η_1 term (5.5), permitting the separate solution of that equation. The solution $x_2^*(t)$ for both families 1 and 2 can be represented as

$$x_2^*(t) = a_0 + a_1 \cos 2\omega t + a_2 \cos 4\omega t + \cdots , \tag{5.6}$$

the dominant terms being the first three in the Fourier series. The reduced variational equation for η_2 takes the form

$$\ddot{\eta}_2 + \left(\theta_0 + 2\sum_{k=1}^{2} \theta_k \cos 2k\tau\right)\eta_2 = 0 \tag{5.7}$$

where $\tau = \omega t$.

Eq. (5.7) is a standard Hill's equation with three independent parameters θ_0 , θ_1 , θ_2 . The exponents and the eigenfunctions for the unstable solutions can now be computed from the series expansions listed in Hayashi [7].

Selected cases have been calculated for Family 2 ($\nu = 2$ and $\nu = 0$) and for Family 1 ($\nu = 0$). The results are summarized in Table II including a comparison with the behavior. In most cases the analysis of the reduced equation explains the observed behavior. That is, "escape" is associated with a real exponent and trapped motion with imaginary exponent. There are two cases of disagreement. For case 4, the exponent is real yet the variational motion is trapped. The explanation is simply that the total energy is below that of the "lip". Mathematically, this means that the neglected nonlinear terms are the strong determinants of trapping here. The other instance is case 10 which has an imaginary exponent and yet in which the solutions "escape". This is a situation where the neglect of the coupling between the η_1 and η_2 equation is invalid. If one examines the η_1 equation alone (uncoupled from η_2),

$$\ddot{\eta}_1 + [1 - 0.1\nu - 0.2x_2^*(t)]\eta_1 = 0, \tag{5.8}$$

TABLE II

Hill's analysis for selected periodic motions of Fig. 12

No.	Family	Detuning ν	*Basic periodic solution* $X_2^*(t)$: Initial conditions from Fig. 12 $X_2(0)$	$\dot{X}_1(0)$	Fourier components a_0	a_1	a_2	Frequency of oscillation ω	*Variational solution* η_2: Parameters θ_i θ_0	θ_1	θ_2	Characteristic exponent (α) and associated dominant eigen functions for real α	Experimental observations and remarks
1	2	2	−0.19	2.4	.033	−.257	.033	0.875	5.47	−1.01	0.12	Imaginary	Slow modulations resembling simple periodic motion. "Trapped" behaviour.
2	2	2	0	6.53	.45	−.65	.20	0.810	10.2	−2.96	0.91	Imaginary	Fast modulations indicating 1/2 subharmonic component. "Trapped" behaviour.
3	2	2	0.185	7.3	.584	−.682	.283	0.795	11.90	−3.24	1.345	Imaginary	As in case 1
4	2	2	−0.796	0.50	−.174	−.648	.026	0.865	3.94	−2.59	0.104	$\alpha = \pm 0.263$ $-0.23 + \sin(2\tau - 21°)$ $-0.21\sin(4\tau - 21°) + \cdots$	As in case 1
5	2	2	−0.810	1.20	−.170	−.67	.030	0.865	3.97	−2.68	0.120	$\alpha = \pm 0.318$ $-0.24 + \sin(2\tau - 21°)$ $-0.22\sin(4\tau - 21°) + \cdots$	Slow modulations resembling simple periodic motion. Eventual "escape."
6	2	0	−0.185	8.40	.457	−.892	.250	0.920	7.95	−3.15	0.885	Imaginary	As in case 1
7	2	0	−0.04	8.80	63	−.93	.26	0.900	9.6	−3.45	0.965	$\alpha = \pm .03$ $.44\sin(\tau - 48°) + \sin(3\tau - 48°)$ $-.21\sin(5\tau - 48°) + \cdots$	Fast modulations and generation of ½ sub-harmonic. Eventual "escape."
8	2	0	0.30	10.30	.875	−.95	.375	0.875	12.0	−3.70	1.46	Imaginary	Slow modulations resembling periodic motion. "Trapped" behaviour.
9	1	0	0.70	3.20	−1	.72	.08	0.96	3.69	2.35	0.261	Imaginary	As in case 1
10	1	0	0.94	4.46	−.123	.969	.094	1.05	2.96	2.64	0.256	Imaginary	Fast modulations. "Possible" generation of 1/2 sub-harmonic cause-Eventual "escape."

for the case at hand it turns out that the exponent for the separated η_1 solution is also imaginary but the solution is very close to a region of primary instability. It is the coupling between η_1 and η_2 to which the instability must be ascribed.

Referring again to Table II, we see that the parameters θ_1 and θ_2 are typically of magnitude 4 or less. Thus instability is associated with values of θ_0 in the neighborhood of 1, 4, 9, 16 etc. The type of modulation seen should be slow for $\theta_0 \simeq 4$, 16 etc. since here the period of the variational function, η_2, is 2π which matches the period of the primary periodic oscillation (cases 4 and 5). However, for $\theta_0 = 1$, 9 etc., the period of the variational function, η_2 , is π so the modulations appear rapid (cases 2 and 7). Note also that while the eigenfunction for case 7 contains a sin τ term and so qualifies as a $\frac{1}{2}$ subharmonic the dominant term is sin 3τ, in keeping with $\theta_0 \simeq 9$.

No cases are shown in Table II for Family 3 periodic motions. To analyze these the $6\omega t$ term has to be included in $x_2^*(t)$ and the resulting Hill's equation has four parameters. The experimentally observed stability regions for this family are quite narrow and the tedious analysis has been omitted.

5.2. Slow modulation analysis. Computer simulation shows that trapped solutions are often characterized by much smaller amplitudes in x_2 than in x_1 . (This does not conflict with the statement in the previous section that for variational solutions η_2 is often much larger than η_1 .) If $|x_2|/|x_1|$ is sufficiently small, the nonlinear term $3x_2^2$ in (2.2b) will be comparable to the other nonlinear terms and a conventional perturbation analysis regarding all nonlinear terms as small can be pursued. This kind of analysis lead to slowly modulated oscillations, and the slowness of modulation is a test of the validity of the section. While $|x_2|$ must be small, $|x_1|$ and the energy of the solution may be quite large.

Eqs. (2.2) are rewritten as

$$(d^2x_1/dt^2) + x_1 = \delta f_1(x_1 , x_2), \tag{5.9a}$$

$$(d^2x_2/dt^2) + 4x_2 = \delta f_2(x_1 , x_2), \tag{5.9b}$$

where

$$\delta f_1(x_1 , x_2) = 0.2x_1x_2 + 0.1\nu x_1 , \tag{5.10}$$

$$\delta f_2(x_1 , x_2) = -3x_2^2 + 0.1x_1^2 , \tag{5.11}$$

and δ is the perturbation parameter.

Several techniques are available for this problem. The one which will be used is the asymptotic expansion of Bogoliubov and Mitropolski [8]. It will be necessary to carry the solution to order δ^2, and this technique proves to be convenient. Principal solutions are taken in the form

$$x_{j0} = R_{0j} \cos (jt + \phi_{0j}), \qquad j = 1, 2 \tag{5.12}$$

where R_{0j} and ϕ_{0j} are slowly varying functions of time. The complete solutions are expansions in δ

$$x_j(t) = x_{j0} + \delta x_{j1} + \delta^2 x_{j2} + \cdots \tag{5.13}$$

where the x_{jk} are functions of R_{0j} and ϕ_{0j} as well as time. The differential equations for R_{0j} and ϕ_{0j} are taken in the form

$$(d/dt)(R_{0j}) = \delta A j_0(R_{0j}, \phi_{0j}) + \delta^2 A j_1(R_{0j}, \phi_{0j}) + \cdots, \qquad j = 1, 2, \tag{5.14}$$

$$(d/dt)(\phi_{0j}) = \delta B_{j0}(R_{0j}, \phi_{0j}) + \delta^2 B_{j1}(R_{0j}, \phi_{0j}) + \cdots, \qquad j = 1, 2. \tag{5.15}$$

The series (5.13) are substituted into (5.9) along with series expansion of the functions f_1 and f_2. Separate equations are formulated for each power of δ. The secular terms that are generated from the nonlinear functions are then eliminated by choice of the functions A_{jm} and B_{jm}. The critical term $3x_2^2$ has no influence on the first approximation solution (A_{j0} and B_{j0}). Accordingly we can use this analysis for larger values of x_2 than might have been supposed originally. The first order set of amplitude and phase variations admit two well-known integral invariants (see [9]). The first of these adiabatic invariants is related to the total energy (which is of course a precise invariant). The second adiabatic invariant is the averaged perturbation Lagrangian. Expressed in terms of R_{0j}, ϕ_{0j} these invariants are

$$R_{01}^2 + 4R_{02}^2 = \text{constant} \underset{=}{\text{def}} \bar{E}_0^2, \tag{5.16}$$

$$R_{01}^2 R_{02} \cos(2\phi_{01} - \phi_{02}) - 4\nu R_{02}^2 = \text{constant}. \tag{5.17}$$

In order to reflect the influence of the quadratic term in x_2, the amplitude and phase variations have to include terms of the order of δ^2. From these equations one can generate an appropriate energy invariant which is

$$R_{01}^2(1 + .025\nu\delta) + 4R_{02}^2 = \text{constant} \underset{=}{\text{def}} E_\theta^2. \tag{5.18}$$

A second invariant can again be obtained reflecting the second-order correction to (5.17). This integral is

$$R_{01}^2 R_{02}(1 + .025\nu\delta)\cos(2\phi_{01} - \phi_{02}) + k_0\delta R_{02}^4 + (k_1\delta - 4\nu)R_{02}^2 = \text{constant} \underset{=}{\text{def}} M', \tag{5.19}$$

where k_0, k_1 are constant depending on ν, E_θ. These are detailed in [10].

As is customary in coupled oscillations of this kind, there is only a single relevant phase variable $(2\phi_{01} - \phi_{02})$ which we may call ψ_0, so that Eqs. (5.18) and (5.19) relate only three variables. Following a transformation used by Gilchrist [11], a new variable χ is defined by

$$\sin\chi = 2R_{02}/E_\theta; \qquad \cos\chi = R_{01}(1 + .025\nu\delta)^{1/2}/E_\theta \tag{5.20}$$

which identically satisfy (5.18). Then (5.19) becomes

$$\sin\chi\cos^2\chi\cos\psi_0 + \frac{\delta k_0 E_\theta}{8}\sin^4\chi + \left(\frac{\delta k_1}{2E_\theta} - \frac{2\nu}{E_\theta}\right)\sin^2\chi = \frac{2M'}{E_\theta^3} \tag{5.21}$$

which is then a single constraint between the two remaining variables χ and ψ_0.

In (5.21) all of the coefficients except M' depend on the system parameter ν, and E_θ. Thus M' may be regarded as the sole relevant initial-condition parameter once E_θ is set. A diagram of integral curves in the $\chi - \psi_0$ plane can be constructed with M' as a parameter, such as Figs. 30, 31. Singular points in this diagram correspond to stationary amplitude and phase—i.e. periodic solutions. A stable singular point such as A or B in Fig. 30 corresponds to stable periodic motions and for initial conditions on a closed trajectory surrounding such a point the motion will be a modulated periodic one. The saddle at C in Fig. 30 is an unstable singular point in that small deviations of initial conditions will produce large excursions of χ and ψ_0, yet interestingly the long-time behavior of these variables is periodic.

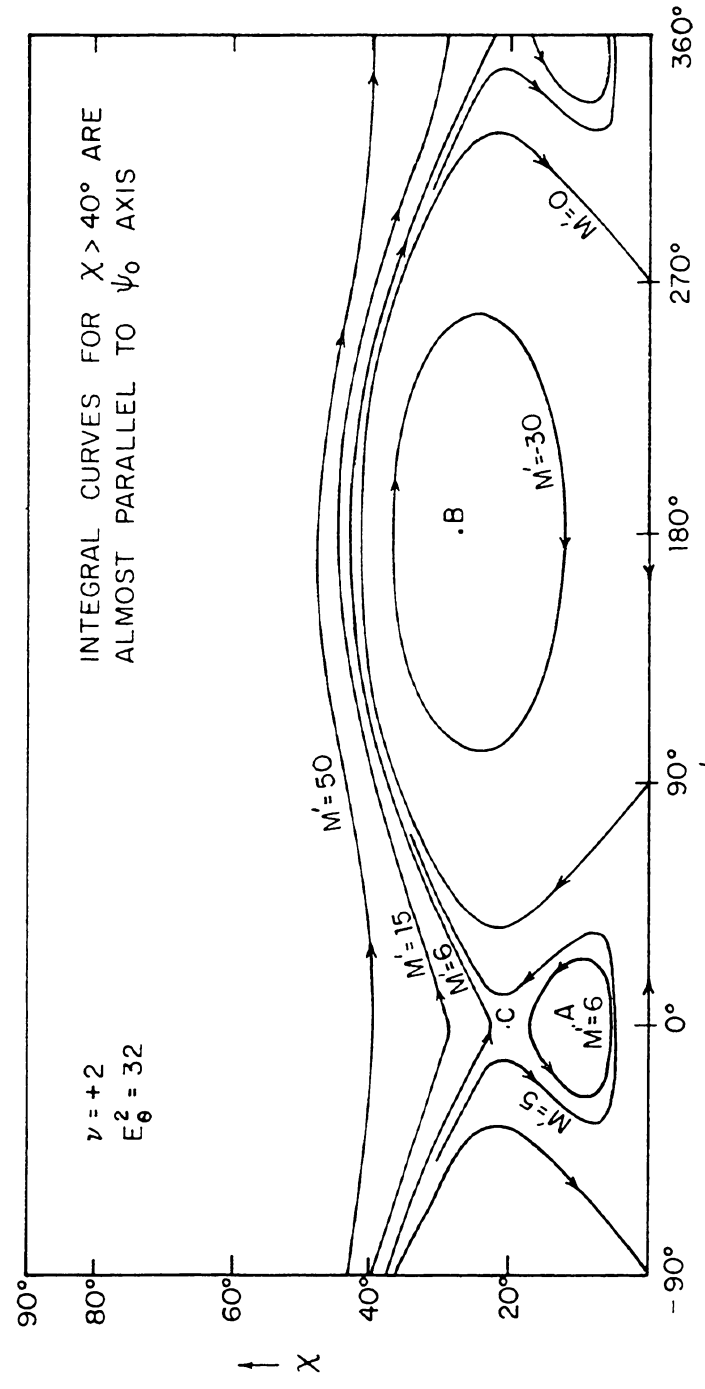

FIG. 30. Integral curves in $\chi - \psi_0$ plane.

The special feature of the present analysis is that the excursions of χ and ψ_0 may be large in these modulated solutions without invalidating the results. The essential restriction is that the modulation must be slow for the results to be valid, and slowness generally

requires sufficiently small x_2. Since $\tan \chi \simeq 2R_{02}/R_{01}$ this means that χ must be less than some critical level χ^* in each diagram. The higher the energy level, the lower χ^* will be.

In Fig. 30 point B corresponds to a Family 1 motion while A and C belong to Family 2.

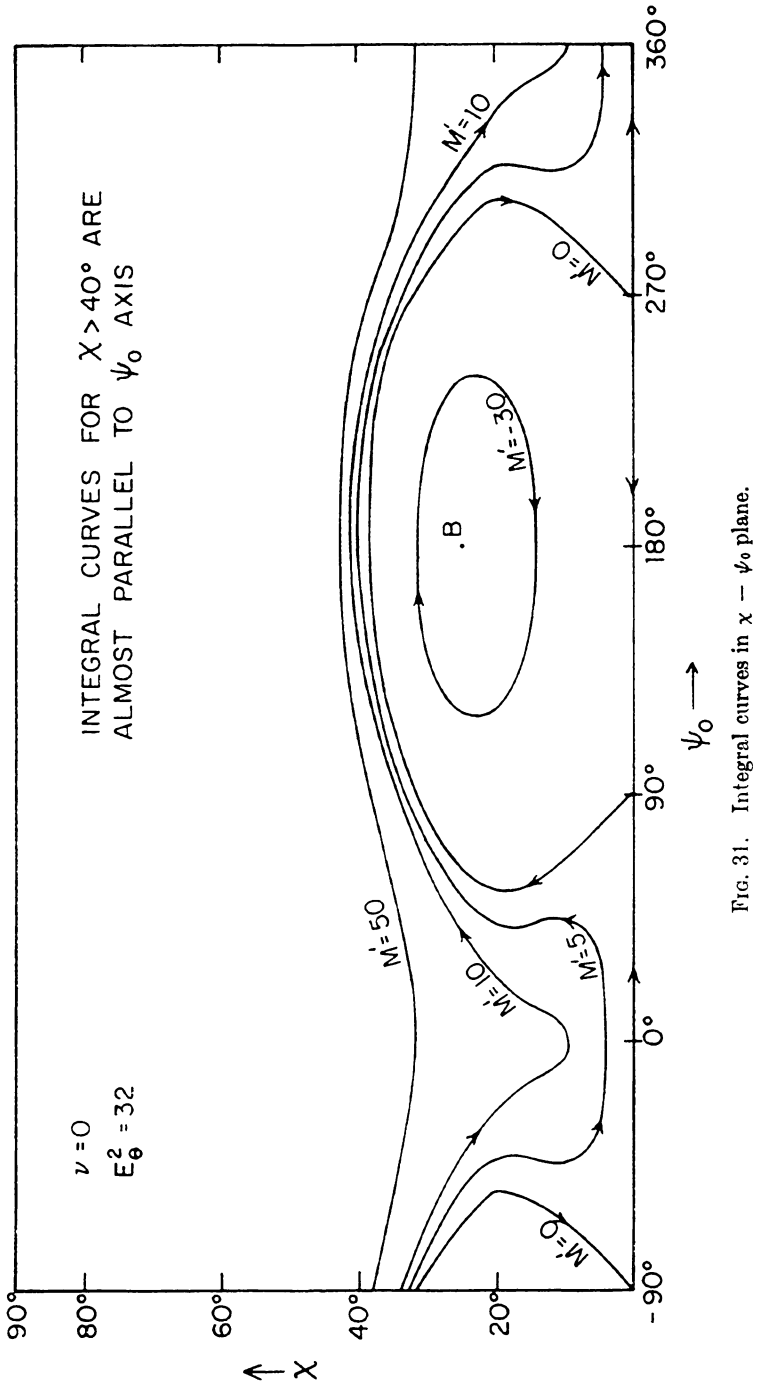

FIG. 31. Integral curves in $\chi - \psi_0$ plane.

For the particular energy level selected the χ corresponding to B and C is so large as to make the analysis marginally valid. B is experimentally observed to be stable for sufficiently small deviations of initial conditions, while C gives rise to escape solutions along the branch of the saddle proceeding toward increasing χ. It is interesting to note that at higher energies the singularity corresponding to B actually develops instability by the modulation frequency rising to one half of the fundamental frequency. Of course the present analysis is invalid well before that occurs.

From Fig. 12 we note that for $\nu \leq 1.3$ there is a band of energies for which only Family 1 solutions exist (e.g. for $\nu = 0$ the band extends from $E_0 = 0$ to $E_0 \simeq 25$). In such cases the singular points A and C are absent as in Fig. 31. The singular points A and C do appear, however, for a much larger value of E_θ^2. The closed contours around A that are then obtained verify again the high-energy trapped solutions seen experimentally (e.g. Fig. 12; Family 2, $\nu = 0$ and $x_2(0) \simeq -.3$). The singular points A and C, when they do exist, always lie on $\psi_0(0) = 0$. For a specified ν, the associated χ coordinate is, however, a function of the energy parameter E_θ^2. In particular the calculations (detailed in [10]) show that for $\nu > 1.3$ the singular points A and C exist from small E_θ^2 upward to large values and with an almost constant spacing of χ. For $1.3 > \nu \geq 1$, A and C approach each other with increasing energy and finally coalescence occurs at some $E_\theta^2 = \bar{E}_\theta^2$. The singular points then *reappear* at an increased value of $E_\theta^2 = \hat{E}_\theta^2 > \bar{E}_\theta^2$ and become spaced further apart with increasing energy. For $\nu < 1$ the singular points do not appear till some high value of energy E_θ^2 and then become spaced further apart with increasing energy. The critical values of R_{01}, R_{02} that correspond to the coalescence condition for a specified ν are easily calculated and may be used to evaluate the corresponding $x_2(0)$ and $\dot{x}_1(0)$ from (5.13). These calculations show that the vertical tangents drawn in Fig. 12 are coincident with the points of coalescence. The correspondence is less accurate at higher energies and this can be attributed to the neglect of terms in the expansion (5.13) beyond x_{i2}.

Note that there are saddle points at $\chi = 0$; $\psi_0 = \pm\pi/2$ in Figs. 30, 31 indicating a periodic solution. This motion, however, corresponds to the initial conditions $\dot{x}_1(0) \neq 0$ and very small $\dot{x}_2(0)$, and is always linearly unstable. Such an initial condition furthermore is not represented in Fig. 12.

6.0. Conclusion. We have considered in this paper a nonlinear dynamical system that exhibits oscillatory motion for small amplitudes and an anticipated divergent behavior in one or both of the coordinates at some large amplitudes. The study has, however, revealed the existence of bands of "trapped" modes having unusually large energies and separated by regions of divergent solutions. These trapped solutions neighbor families of periodic motions which form a two-dimensional subspace in the four-dimensional phase space.

The stability transition of these conservative periodic motions (based on a linearized analysis) corresponds to the two cases of the characteristic exponent of the system of Hill's equations having either a zero exponent or an imaginary part of π/T. The latter case corresponds to the generation of a subharmonic component of order $\frac{1}{2}$ and the experimental results indicate both of the above transitions.

Another interesting observation has been the nature of the "escape" path relative to the position of the "lip." It has been found that the "escape" trajectory (for an initial velocity in the x_1 coordinate) does not in general pass over the "lip" but instead follows a displaced path.

The results obtained here have been for a truly conservative system. To make the results meaningful in engineering problems, a consideration of the effects of small dissipation must be included. In particular, it would be interesting to know whether, and under what conditions, it may be possible for the motions to decay from a high-energy trapped state to rest. This would be especially significant when no continuous band of trapped solutions exists down to the rest state. This study will be described in Part II of this paper.

References

[1] B. Budiansky, *Dynamic buckling of elastic structures: criteria and estimates*; in *Dynamic stability of structures*, Proc. Internat. Conference Northwestern University, Evanston, Illinois, 1965

[2] G. Contopoulos, *A third integral of motion in a galaxy*, Z. Astrophys. **49**, 273–291 (1960)

[3] M. Hénon and C. Heiles, *The applicability of the third integral of motion: some numerical experiments*, Astronom. J. **69**, 73–79 (1964)

[4] G. Contopoulos and J. D. Hadjidemetriou, *Characteristics of invariant curves of plane orbits*, Astronom. J. **73**, 86–96 (1968)

[5] G. Contopoulos, *Orbits in highly perturbed dynamical systems. I. Periodic orbits*, Astronom. J. **75**, 96–107 (1970)

[6] H. Poincaré, *Les méthodes nouvelles de la méchanique céleste*, Tomes 1, 2, 3, Paris, 1892, 1893, 1899; reprint, Dover, New York, 1957; English transl., NASA TTF-450, 451, 452, National Aeronautics and Space Administration, Washington, D. C., 1967

[7] C. Hayashi, *Nonlinear oscillations in physical systems*, McGraw-Hill, New York, 1964

[8] N. N. Bogoljubov and Ju. A. Mitropol'skiĭ, *Asymptotic methods in the theory of non-linear oscillations*, Fizmatgiz, 1958; English transl., Hindustan, Delhi; Gordon and Breach, New York, 1962

[9] R. E. Kronauer and S. A. Musa, *Exchange of energy between oscillations in weakly nonlinear conservative systems*, J. Appl. Mech. **33**, 451–452 (1966)

[10] R. Subramanian, *Escape from a potential well*, Ph.D. Dissertation, Harvard University, Cambridge, Mass., 1970

[11] A. O. Gilchrist, *The free oscillations of conservative quasi-linear systems with two degrees of freedom*, Internat. J. Mech. Sci. **3**, 286–311 (1961)